Molecular Plant Pathology

WILEY

ORIGINAL ARTICLE OPEN ACCESS

Negative Immune Regulator CAD7 Functions as a Small-Molecule Aldehyde Reductase and Increases Histamine Accumulation in Arabidopsis

Liwen Ding[1] | Zewen Liu[1] | Weihang Wang[1] | Yang Yang[2] | Ren Sa[1] | Hongmei Wang[1] | Liru Mi[1] | Yalan Qin[1] | Shaocong Kang[1] | Meruyert Medelbek[3] | Assiya Ansabayeva[3] | Yuling Meng[1] | Weixing Shan[1]

[1]State Key Laboratory of Crop Stress Resistance and High-Efficiency Production and College of Agronomy, Northwest A&F University, Yangling, Shaanxi, China | [2]State Key Laboratory of Crop Stress Resistance and High-Efficiency Production and College of Plant Protection, Northwest A&F University, Yangling, Shaanxi, China | [3]Department of Agronomy, A. Baitursynov Kostanay Regional University, Kostanay, Republic of Kazakhstan

Correspondence: Weixing Shan (wxshan@nwafu.edu.cn)

Received: 22 May 2025 | **Revised:** 7 December 2025 | **Accepted:** 12 December 2025

Keywords: cinnamyl alcohol dehydrogenase7 | histamine | *Phytophthora parasitica* | plant susceptibility | small-molecule aldehyde reductase

ABSTRACT

Negative immune regulator CAD7 is a non-canonical member of the CAD (cinnamyl alcohol dehydrogenase) family in plants. However, little is known on its biochemical functions and underlying mechanisms of immune regulation. Here, we show that *Arabidopsis thaliana* AtCAD7 harbours substrate-binding residues divergent from lignin-forming CADs (AtCAD4/5), being conserved with bacterial alcohol dehydrogenases EcYahK and EcYjgB. Comparative enzymatic analysis revealed that AtCAD7 exhibits a broad substrate preference for diverse small-molecule aldehydes, including histamine-derived intermediates, being distinct from the canonical lignin-forming AtCAD5. Metabolomic analyses revealed that *AtCAD7*-overexpression transformants were affected in the biosynthesis and metabolism of amino acids, whereas *AtCAD7*-silencing lines were activated in the phenylpropanoid pathway and increased in flavonoid accumulation. Histamine was elevated in *AtCAD7*-overexpression lines and functional validation revealed its promoted effect on plant susceptibility to *Phytophthora parasitica*. In contrast, phytoalexins scopolin and chlorogenic acid were enriched in *AtCAD7*-silencing lines, accompanied by upregulated expression of phenylpropanoid pathway-related genes. Functional validation demonstrated that scopolin and chlorogenic acid enhanced plant resistance to *P. parasitica*. Collectively, our study uncovers that CAD7 functions as a metabolic hub linking small-molecule aldehyde reductase activity to immune suppression, providing a potential novel target for developing crops with enhanced resistance to *Phytophthora* pathogens.

1 | Introduction

Cinnamyl alcohol dehydrogenase (CAD) is of particular significance in monolignol biosynthesis as it catalyses the final step of this process, converting hydroxycinnamyl aldehydes into their corresponding alcohols (Gross et al. 1973; Mansell et al. 1974). CAD homologues, encoded by a multigene family, are found in various organisms, including bacteria and eukaryotes (Barakat et al. 2009; Kim et al. 2004, 2007; Larroy et al. 2002). The *Arabidopsis* genome encodes nine *CAD* homologues (*AtCAD1-9*), all containing conserved Zn^{2+}-binding and NADPH-binding domains (Kim et al. 2004). However, only AtCAD4 and AtCAD5 have been confirmed to have significant activity against cinnamyl aldehydes (Kim et al. 2004), while AtCAD7 and AtCAD8 have markedly undetectable catalytic efficiency (Kim et al. 2004). Tissue-specific expression

Liwen Ding and Zewen Liu are contributed to the work equally.

studies and enzyme kinetic characterisation indicate that the *CAD* family members exhibit distinct expression patterns and substrate specificities. These results suggest that they may play diverse roles in plant development (Barakat et al. 2009; Kim et al. 2004, 2007).

The CAD family is recognised to be associated with lignin biosynthesis, but emerging evidence indicates that significant functional diversification has occurred in plants, with certain members evolving roles in stress-responsive metabolism (Wu et al. 2024). Phylogenetic analysis indicates that the CAD7 subfamily is highly expanded in plant genomes, suggesting evolutionary selection for their specialised functions (Li et al. 2019). Consistent with this neofunctionalisation paradigm, the expression of *AtCAD7* and *AtCAD8* is induced by biotic stresses, including *Pseudomonas syringae* and *Phytophthora* infections (Kiedrowski et al. 1992; Li et al. 2019). CAD7 subfamily members, including AtCAD7 and its *Nicotiana benthamiana* ortholog NbCAD7, have been identified to be targeted by multiple Avr3a-like effectors from several *Phytophthora* species (Li et al. 2019). Furthermore, CAD7 has been shown to suppress multiple pattern-triggered immunity (PTI) responses, including callose deposition and the reactive oxygen species (ROS) burst (Li et al. 2019). Biochemical studies revealed their divergence from canonical lignin-forming CADs. For example, AtCAD8 (ELI3-2) displays activity toward non-lignin aldehydes such as 2-methoxybenzaldehyde and salicylaldehyde (Somssich et al. 1996). A closely related potato CAD-like protein, defence-related alcohol dehydrogenase (DRD-1), is also strongly induced by infection or wounding and exhibits broad specificity toward aromatic and aliphatic aldehydes with the highest affinity toward 2-methoxybenzaldehyde, salicylaldehyde and hexanal (Montesano et al. 2003). Notably, recent studies have uncovered a pivotal role of AtCAD7 (named cinnamaldehyde and hexenal reductase) in green leaf volatiles (GLVs) metabolism, where it converts (*Z*)-3-hexenal to (*Z*)-3-hexen-1-ol during wound-induced GLV bursts. This enzymatic activity fine-tunes the balance between toxic aldehydes and predator-attracting alcohols, optimising indirect herbivore defence (Tanaka et al. 2018). Such functional plasticity spanning its roles in pathogen response, herbivore deterrence, and volatile signalling highlights the CAD7 subfamily as a metabolic nexus in plant stress adaptation. However, the biochemical mechanisms underlying AtCAD7 function in secondary metabolism and immune suppression remain enigmatic.

Several secondary metabolites play crucial roles in plant disease resistance. The phenylalanine metabolic pathway, for instance, is involved not only in the synthesis of secondary metabolites such as lignin (Liu et al. 2018), flavonoids (Jun et al. 2018) and phenols (Chen et al. 2006), but also in the production of salicylic acid (SA), an important hormone closely linked to plant disease resistance (Kim and Hwang 2014). Many metabolites act as signalling molecules that mediate communications within and between species and control various metabolic and physiological processes in both pathogens and their host plants (Baker and Rutter 2023). Histamine is a pivotal biological signalling molecule and exhibits diverse activities in numerous pathological and physiological contexts (Jutel et al. 2009). Multiple studies have reported that pathogenic bacteria, such as *Pseudomonas aeruginosa*, can induce host cells to produce and release histamine (Abraham and Malaviya 1997; Chonmaitree et al. 1994; Ono et al. 2019; Tsai et al. 2015; Xu et al. 2012).

Oomycetes are eukaryotic diploid filamentous microorganisms that are similar in morphology to, but phylogenetically distant from, true fungi (Thines 2018). Many oomycetes are plant pathogens, affecting various herbaceous and woody plants and causing significant economic losses and ecological disturbances around the world (Barwell et al. 2021; Fones et al. 2020). A notable example is the late blight pathogen *Phytophthora infestans*, the cause of the Irish potato famine, and it remains the most devastating pathogen of potato and tomato (Fones et al. 2020; Ristaino et al. 2021). Use of genetic resistance is the most effective strategy to control diseases. However, oomycetes are notorious for overcoming host genotype-specific resistance, leading to the heavy reliance on fungicide application for the control of many oomycete diseases (Saraiva et al. 2023). Understanding molecular mechanisms underlying plant susceptibility to oomycetes is crucial for developing effective disease control strategies.

AtCAD7 has been identified as a negative regulator of plant immunity against *Phytophthora* species (Li et al. 2019). However, the relationship between its biochemical functions and plant immunity remains poorly understood. In this study, we analysed the biochemical basis and functionality of AtCAD7 in negative regulation of plant immunity. Our sequence alignment and enzymatic activity assays showed differential substrate-binding residues of AtCAD7 from those of canonical CADs but which are close to those found in the bacterial *Escherichia coli* dehydrogenases EcYahK and EcYjgB, both of which have catalytic activities for small molecule aldehydes. Metabolomic profiling of *AtCAD7*-overexpressing and *AtCAD7*-silenced transformants uncovered its distinct secondary metabolism and association in immune function. *AtCAD7* overexpression enhances plant susceptibility, primarily through elevated histamine accumulation. In contrast, silencing *AtCAD7* activates immune-related metabolic processes, leading to the accumulation of scopolin and chlorogenic acid, which promote disease resistance against *Phytophthora parasitica*. Our findings highlight the evolutionary plasticity of CAD7 enzymes and provide new insights into leveraging plant–pathogen interactions for sustainable agriculture.

2 | Results

2.1 | AtCAD7 Shares Conserved Catalytic Sites With Bacterial Alcohol Dehydrogenases

AtCAD7 belongs to the CAD family, yet its cinnamyl alcohol dehydrogenase activity is not strongly active (Kim et al. 2004). To identify its potential catalytic substrates, we performed sequence alignment of AtCAD7 against structurally related dehydrogenases using BLAST. Comparative analysis revealed sequence identities of AtCAD7 with AtCAD4 and AtCAD5 (46%), sinapyl alcohol dehydrogenase (70%), mannitol dehydrogenase (72%), nerolidol dehydrogenase (63%) and 10-hydroxygeraniol dehydrogenase (69%) (Figure 1a). Compared with alcohol dehydrogenases, AtCAD7 exhibits significant differences in substrate-binding residues, which indicate that it has distinct catalytic specificity.

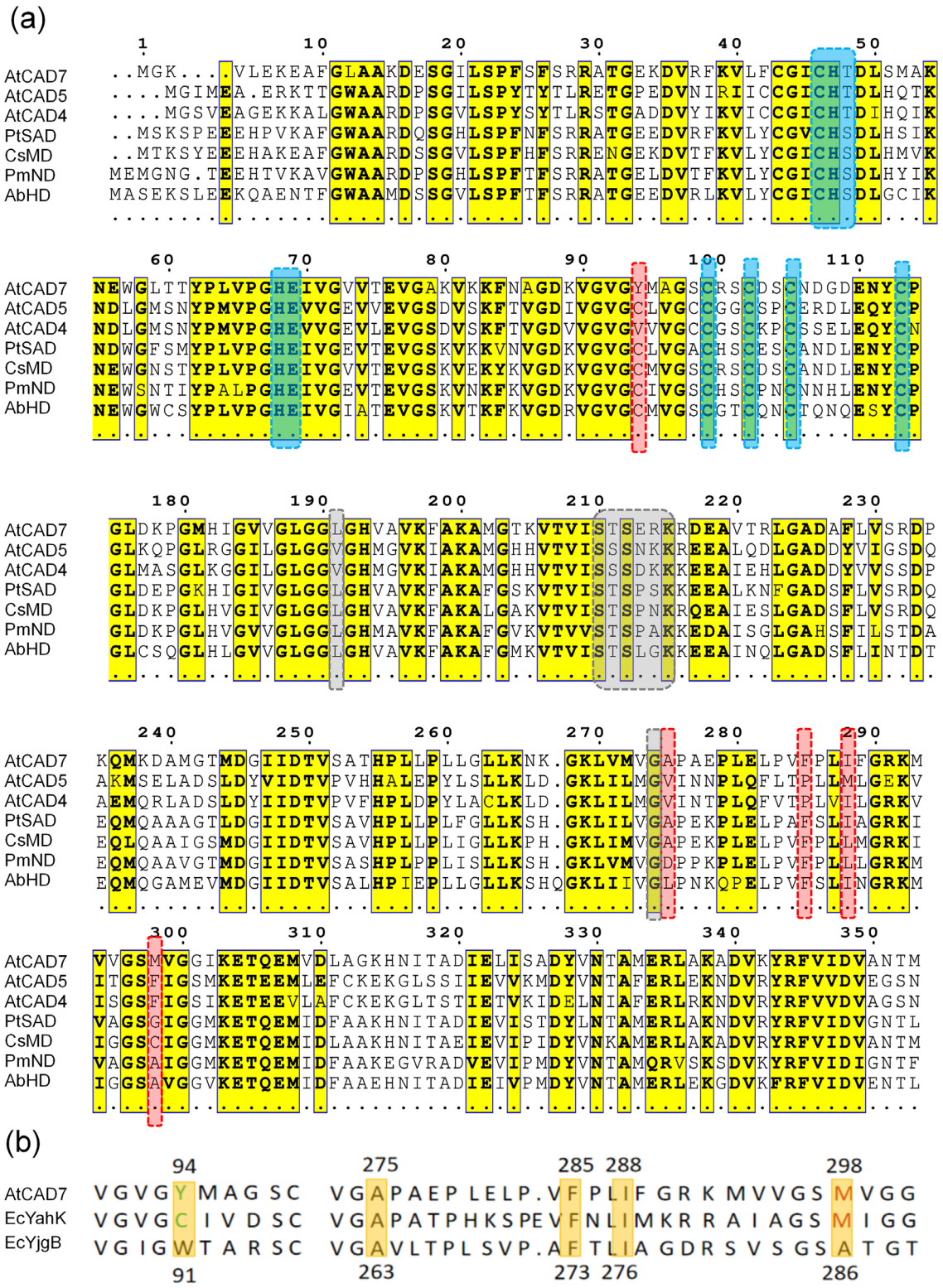

FIGURE 1 | Sequence alignment analysis of the dehydrogenase family proteins to identify functionally critical catalytic residues in AtCAD7. (a) Sequence alignments of AtCAD7 with cinnamyl alcohol dehydrogenase AtCAD5, AtCAD4, sinapyl alcohol dehydrogenase of *Populus tremuloides* (PtSAD), mannitol dehydrogenase of *Cannabis sativa* (CsMD), nerolidol dehydrogenase of *Persicaria minor* (PmND), and 10-hydroxygeraniol dehydrogenase of *Atropa belladonna* (AbHD). Blue frames indicate conserved residues involved in the Zn^{2+}-binding. Grey frames denote residues involved in the $NADP^{+}$-binding. Pink frames indicate substrate binding sites. (b) Sequence alignment of AtCAD7 with the substrate binding sites of *Escherichia coli* dehydrogenases YahK and YjgB. The residues crucial for substrate specificity are marked by yellow boxes.

Sequence alignment showed that the AtCAD7 substrate binding sites were similar to the *Escherichia coli* dehydrogenases EcYahK and EcYjgB (43%) (Figure 1b), particularly at the Met298 residue critical for substrate recognition (Bomati and Noel 2005). Both EcYahK and EcYjgB are NADPH-dependent alcohol dehydrogenases that catalyse the reduction of many small aromatic rings and short CH chain aldehydes to the corresponding alcohols, with NADPH as a cofactor and have broad specificity toward aldehyde substrates (Nguyen et al. 2020; Pick et al. 2013).

Structural studies have shown that the catalytic active site of EcYjgB includes Ile276, Ala263/286, Trp91, Phe273, and the nicotinamide ring of NADP, in which the aromatic side chains Phe273 and Trp91 play a critical role in holding substrates and conferring broad selectivity (Nguyen et al. 2020). The sequence of AtCAD7 is consistent with three of the key active sites (Ile276, Ala263, and Phe273) of EcYjgB, except for Trp91 and Ala286. The substrate key active site Met298 in AtCAD7 aligns with EcYahK but differs from EcYjgB (Figure 1b). Therefore, AtCAD7 may also have a wide range of substrates.

2.2 | AtCAD7 Catalyses a Wide Range of Small Aldehydes

EcYjgB exhibits higher catalytic efficiency toward unbranched short-chain aliphatic aldehydes and aromatic aldehydes (Pick et al. 2013), whereas EcYahK preferentially catalyses branched aldehydes (Pick et al. 2013). This divergence arises from structural differences in their active sites. EcYjgB features a narrow hydrophobic channel formed by a tryptophan residue (Trp91) in its substrate-binding pocket, favouring linear substrates, whereas EcYahK contains a cysteine residue (Cys88) that creates a more spacious cavity accommodating branched and polar groups (Pick et al. 2013). Sequence alignment revealed that AtCAD7 harbours a tyrosine residue (Tyr94) at the analogous position in its substrate-binding site, distinct from both EcYjgB and EcYahK (Figure 1b). The side chain of tyrosine, intermediate in size between tryptophan and cysteine, likely endows AtCAD7 with a unique substrate preference distinct from both *E. coli* enzymes.

To investigate the differences in substrate preferences between AtCAD7 and *E. coli* enzymes EcYjgB and EcYahK, we expressed and purified their recombinant proteins from *E. coli*, with protein integrity confirmed by SDS-PAGE analysis (Figure S1). We selected a set of substrates, including the reported substrates of AtCAD7 homologue AtCAD8 (Somssich et al. 1996), for testing. The substrates included the unbranched (acrolein) and branched aliphatic aldehydes (2-methylbutanal and isovaleraldehyde), aromatic aldehydes (benzaldehyde), branched aromatic aldehydes (2-methoxybenzaldehyde and 3-methoxybenzaldehyde), and polar-group-containing salicylaldehyde. We included its known substrate (*Z*)-3-hexenal (Tanaka et al. 2018) as a positive control, and the inactive substrate *p*-coumaraldehyde (Kim et al. 2004) and the substrate solvent and the absence of substrate as negative controls. The results showed that AtCAD7 exhibited significant aldehyde reductase activity, with NADPH as a cofactor, against acrolein, methylbutanal, isovaleraldehyde, benzaldehyde, 2-methoxybenzaldehyde, 3-methoxybenzaldehyde and salicylaldehyde, compared to the positive and negative controls (Figure 2).

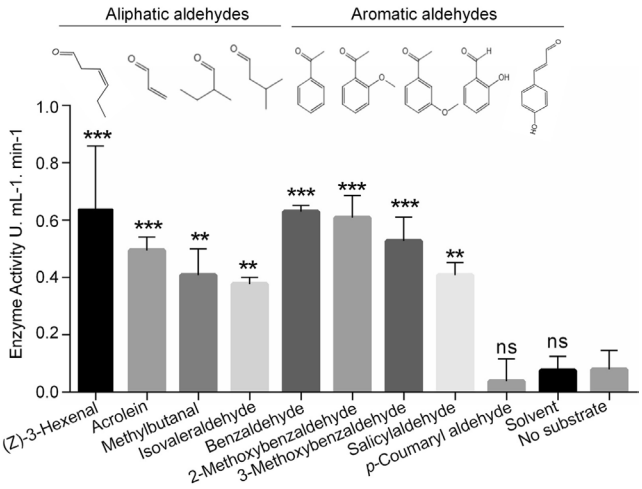

FIGURE 2 | Substrate specificity of small-molecule aldehyde reductase AtCAD7. The enzymatic activity of recombinant AtCAD7 was quantitatively analysed by spectrophotometry using nine different aldehydes as substrates, namely aliphatic aldehydes: (*Z*)-3-hexenal, acrolein, methylbutanal, and isovaleraldehyde; and aromatic aldehydes: benzaldehyde, 2-methoxybenzaldehyde, 3-methoxybenzaldehyde, salicylaldehyde, and *p*-coumaryl aldehyde. Structural formulas of the respective compounds are shown above the bars. Two negative controls were included: solvent (the solvent of substrates) and no substrate. Purified AtCAD7 protein was used, and catalytic rates were measured under standardised reaction conditions. Data represent the mean ± SD of triplicate biological replicates. Statistical significance was assessed by Student's *t* test (**$p < 0.01$, ***$p < 0.001$, ns, not significant).

To further refine the experimental controls in the AtCAD7 enzymatic activity assay, we selected three representative substrates, (*Z*)-3-hexenal, acrolein and salicylaldehyde. The assay was conducted under identical standard enzymatic reaction conditions, with two negative controls included, heat-denatured AtCAD7 protein and that without AtCAD7 protein. Compared with the positive control, heat-denatured AtCAD7 protein showed a significant reduction in activity, while no enzymatic activity was detected in the absence of AtCAD7 (Figure S2a). To verify cofactor specificity, the effects of NADPH and NADH were compared under the same conditions, with results confirming that the reaction of AtCAD7 is specifically dependent on NADPH (Figure S2a). Figure S2b depicts the reaction progress curve of AtCAD7 with the substrate (*Z*)-3-hexenal over 30 min under standard enzymatic activity conditions. The reaction products were further validated by thin-layer chromatography (TLC) using salicylaldehyde and 2-methoxybenzaldehyde as two representative substrates. TLC profiles confirmed the enzymatic conversion of salicylaldehyde to salicylalcohol and 2-methoxybenzaldehyde to 2-methoxybenzyl alcohol (Figure S3).

To clarify the differences in substrate preference within the CAD family proteins and between AtCAD7 and the *E. coli* enzymes EcYjgB and EcYahK, we expressed and purified four recombinant proteins: AtCAD7, AtCAD5, EcYahK and EcYjgB (Figure S4a). Their enzymatic activity assays toward five

substrates ((*Z*)-3-hexenal, acrolein, isovaleraldehyde, salicylaldehyde and *p*-coumaryl aldehyde) showed significant divergence in substrate preferences among the four enzymes, which is consistent with their structural differences in the substrate-binding pocket.

Because EcYjgB prefers unbranched short chain aliphatic aldehydes (Pick et al. 2013), it exhibits higher activity toward acrolein. EcYahK prefers branched aldehydes and consistently showed higher activity toward isovaleraldehyde, salicylaldehyde and *p*-coumaraldehyde (Figure S4b). As a typical cinnamyl alcohol dehydrogenase associated with lignin biosynthesis, AtCAD5 exhibits high activity toward *p*-coumaraldehyde (a lignin precursor) (Kim et al. 2004), but showed relatively low activity toward other non-lignin substrates (Figure S4b). While AtCAD7 exhibits activity toward a variety of substrates, its activities were slightly lower than that of EcYjgB toward the short chain aliphatic aldehydes, lower than that of EcYahK toward the branched isovaleraldehyde and salicylaldehyde, and extremely low toward *p*-coumaraldehyde (Figure S4b). These results indicate that AtCAD7 is functionally divergent from typical cinnamyl alcohol dehydrogenases.

Collectively, these results demonstrate that AtCAD7 is a non-traditional cinnamyl alcohol dehydrogenase and can catalyse a variety of small molecule aldehydes with aromatic rings and aliphatic groups. This not only corroborates its role in GLV metabolism but also expands the known substrate repertoire of AtCAD7 by demonstrating its capacity to catalyse diverse aromatic (salicylaldehyde) and aliphatic (2-methylbutanal) aldehydes, further highlighting its functional versatility.

2.3 | AtCAD7 Is Involved in Regulating Changes in Plant Metabolites

The broad range of substrates of alcohol dehydrogenases in *E. coli* might assist cell survival under oxidative stress (Nguyen et al. 2020; Pick et al. 2013). AtCAD7 has a wide range of substrates in plants, similar to stress-responsive aldehyde dehydrogenases (ALDHs) (Singh et al. 2013), and thus may play an important role in plant stress responses. To explore the metabolic regulatory role of *AtCAD7* in plants, we conducted an unbiased global metabolic profiling using UPLC–MS/MS on three independent *AtCAD7*-overexpressing (OE7-1, OE7-2, OE7-3) and two independent *AtCAD7*-silenced (Ri7-1, Ri7-2) lines and the control wild-type Col-0 (WT) plants. Global metabolomic profiling was performed on three biological replicates per genotype (WT, OE7, Ri7). A total of 654 metabolites were detected.

We established orthogonal partial least squares-discriminant analysis (OPLS-DA) models for OE7, Ri7 and WT to identify differential metabolites (Figure S5a). Compared with principal component analysis (PCA), this method more effectively amplifies intergroup distinctions and demonstrates enhanced performance in screening weakly correlated metabolites (Thévenot et al. 2015). We calculated the R^2 and Q^2 values of the stochastic model to ensure model reliability and prevent overfitting. The results, with p-values < 0.05 (Figure S5b), indicated good model quality. We screened differential metabolites based on OPLS-DA results by using Variable Importance in Projection (VIP) values. Additionally, we combined p-values and fold changes from univariate analysis for further screening. The top 20 differential metabolites ranked by VIP values are shown in Tables S1 and S2.

Metabolites specifically found in OE7 compared to the WT mainly belonged to the organic acids, nucleotides, amino acids and phenolic acids. Metabolites up-regulated in Ri7 compared to the WT mainly included phenolic acids, alkaloids, amino acids and derivatives, lipids, tannins, lignans and coumarins. We used the unit variance scaling normalisation process to visualise the results of these differential metabolites to facilitate detection of changes in metabolites (Figure 3a).

According to the results of differential metabolites, we performed KEGG pathway enrichment analyses. The common pathways in OE7 and Ri7 were biosynthesis and metabolism of amino acids and aminoacyl tRNA biosynthesis. Pathways significantly altered in the Ri7 lines were secondary metabolites in the phenylpropanoid and flavonoid biosynthesis pathways. In the OE7 lines, changes in the biosynthesis pathways of valine, leucine and isoleucine and the metabolism pathways of pyruvate, pyrimidine, β-alanine and 2-oxocarboxylic acid were notable (Figure 3b).

We have shown that AtCAD7 can catalyse the reduction of small-molecule aldehydes to alcohol (Figure 2), and alcohols can be further transformed to produce phenolic acids, ketones and esters, with many of these products being precursors in the amino acid metabolism. The findings align with the results of AtCAD7 metabolomics. Many up-regulated metabolites were identified in OE7 lines, including amino acids and their derivatives, lignans and phenolic acids.

2.4 | *AtCAD7*-Overexpression Increases Histamine Levels and Suppresses Plant Immunity

We conducted a comparative analysis of up-regulated small-molecule metabolites in OE7 lines to investigate the negative regulatory role of *AtCAD7* in plant immunity and its potential involvement in modulating pathogen-facilitative signalling molecules. Among the top 20 small-molecule metabolites, histamine was identified to be a compound with important functions in microbes, plants and animals (Heidarzadeh-Asl et al. 2024; Wang et al. 2021) and was elevated in OE7 lines (Table S1). Consistent with the results of metabolomic profiling, liquid chromatography tandem mass spectrometry (LC–MS/MS) analysis showed 3–6 times higher histamine content in the *AtCAD7*-overexpression line OE7 than that in the WT (Figure 4a). While the role of histamine in plants remains underexplored, its catabolism routes have been identified in plants by KEGG pathway analysis (Kanehisa et al. 2021). Histamine is notably involved in two aldehyde intermediates, methylimidazole acetaldehyde and imidazole-4-acetaldehyde (Figure 4b), suggesting that AtCAD7 might function in the reduction of these two intermediates. Due to limited commercial availability of these two aldehydes, we tested structurally analogous compounds (1-methylimidazole-4-carboxaldehyde and imidazole-4-carbaldehyde) (Figure 4c), with acrolein, salicylaldehyde and (*Z*)-3-hexenal (Tanaka et al. 2018) as the positive controls, and substrate solvent and that without substrate as negative controls. In vitro enzymatic activity assays confirmed that AtCAD7 exhibited

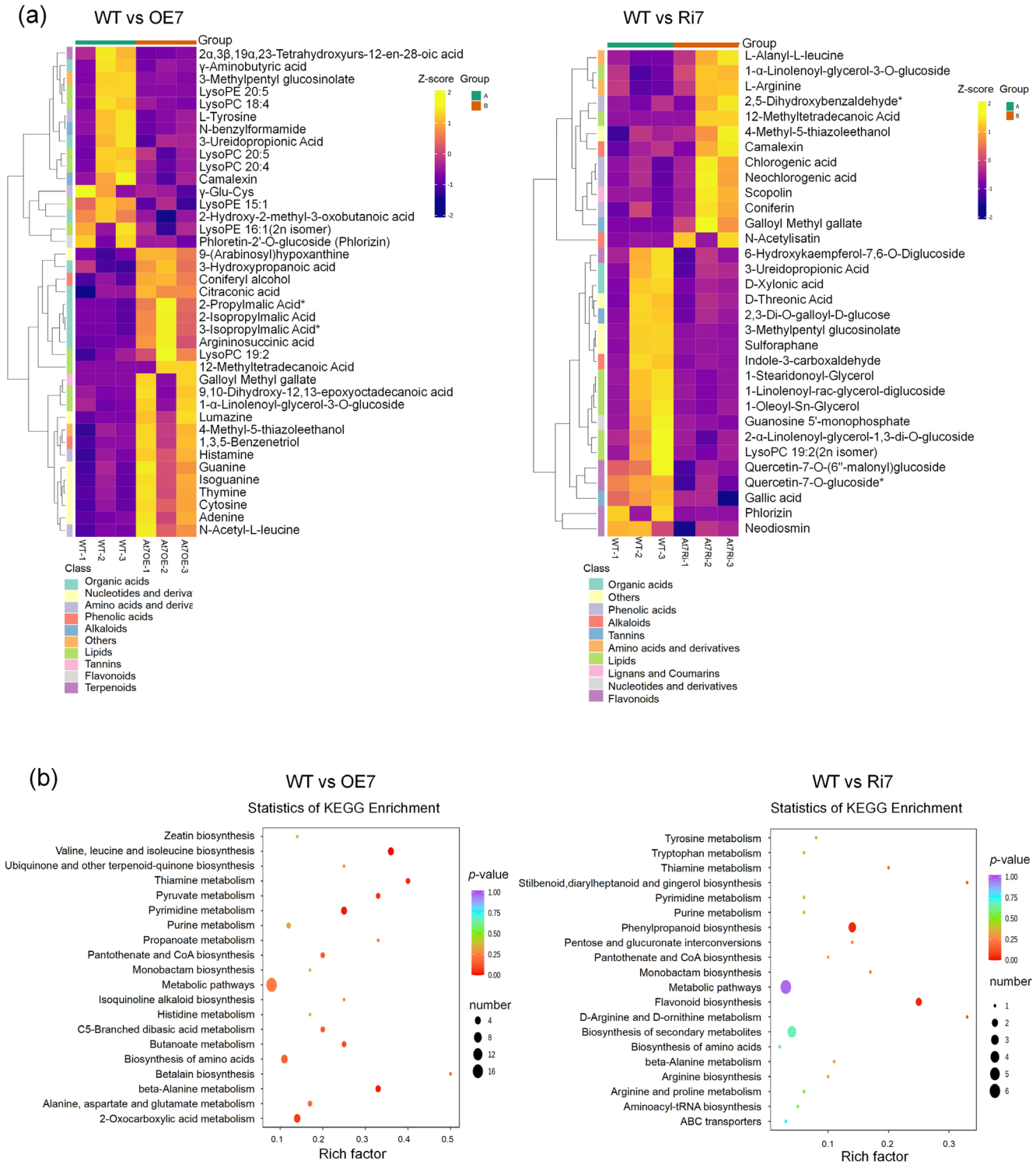

FIGURE 3 | Analysis of differential metabolites between *AtCAD7*-overexpression (OE7) and *AtCAD7*-silenced (Ri7) *Arabidopsis thaliana* transformants. (a) Heat maps showing the clustering of differentially expressed metabolites in the disease-susceptible OE7 lines and disease-resistant Ri7 lines, compared to the wild type (WT) Col-0. The horizontal axis represents samples, while the vertical axis indicates differential metabolite information. The clustering tree on the left represents the hierarchical clustering of these metabolites. Differential metabolites were classified, and their relative abundances were normalised for visualisation: yellow and purple denote high and low levels, respectively. (b) Up-regulated differentially enriched metabolites by KEGG analysis. The horizontal coordinate indicates the rich factor of each pathway, the vertical coordinate is the name of the pathway, and the colour of the dot is the *p*-value; the redder it is, the more significant the enrichment. The size of the dots represents the number of differential metabolites enriched.

catalytic activity toward 1-methylimidazole-4-carboxaldehyde and imidazole-4-carbaldehyde (Figure 4d), indicating that it has the ability to process histamine-derived aldehydes.

Histidine decarboxylase (HDC) acts as the rate limiting enzyme in the histamine biosynthesis pathway and catalyses the conversion of histidine to histamine (Huang et al. 2018). Its activity and expression are regulated by factors such as substrates, products and inhibitors (Kelley et al. 1977; Kollonitsch et al. 1978; Moriguchi and Takai 2020; Wu et al. 2008). The consumption of aldehyde intermediates may relieve feedback inhibition on HDC, thereby increasing production of histamine. To investigate the effects of 1-methylimidazole-4-carboxaldehyde and imidazole-4-carbaldehyde on histidine decarboxylase HDC in plants, we transiently expressed *NbHDC* constructs as N-terminal GFP fusions in *Nicotiana benthamiana* leaves, followed by treatment with these two compounds. NbHDC protein levels were then determined by using a plant histidine decarboxylase ELISA detection kit (MEIMIAN). The results showed that the 1-methylimidazole-4-carboxaldehyde and imidazole-4-carbaldehyde both significantly reduced NbHDC protein levels compared to the negative substrate solvent control (Figure S6a). Therefore, the small molecule aldehyde reductase activity of AtCAD7 can reduce histamine-derived aldehyde intermediates (1-methylimidazole-4-carboxaldehyde and imidazole-4-carbaldehyde) to their corresponding alcohols and disrupt feedback inhibition exerted on HDC (Figure 4b), thus altering histamine metabolic process and leading to increased histamine accumulation in *AtCAD7*-overexpression lines.

Arabidopsis thaliana leaves treated with exogenous histamine showed enhanced disease symptoms compared with the mock control, and pathogen biomass quantification consistently

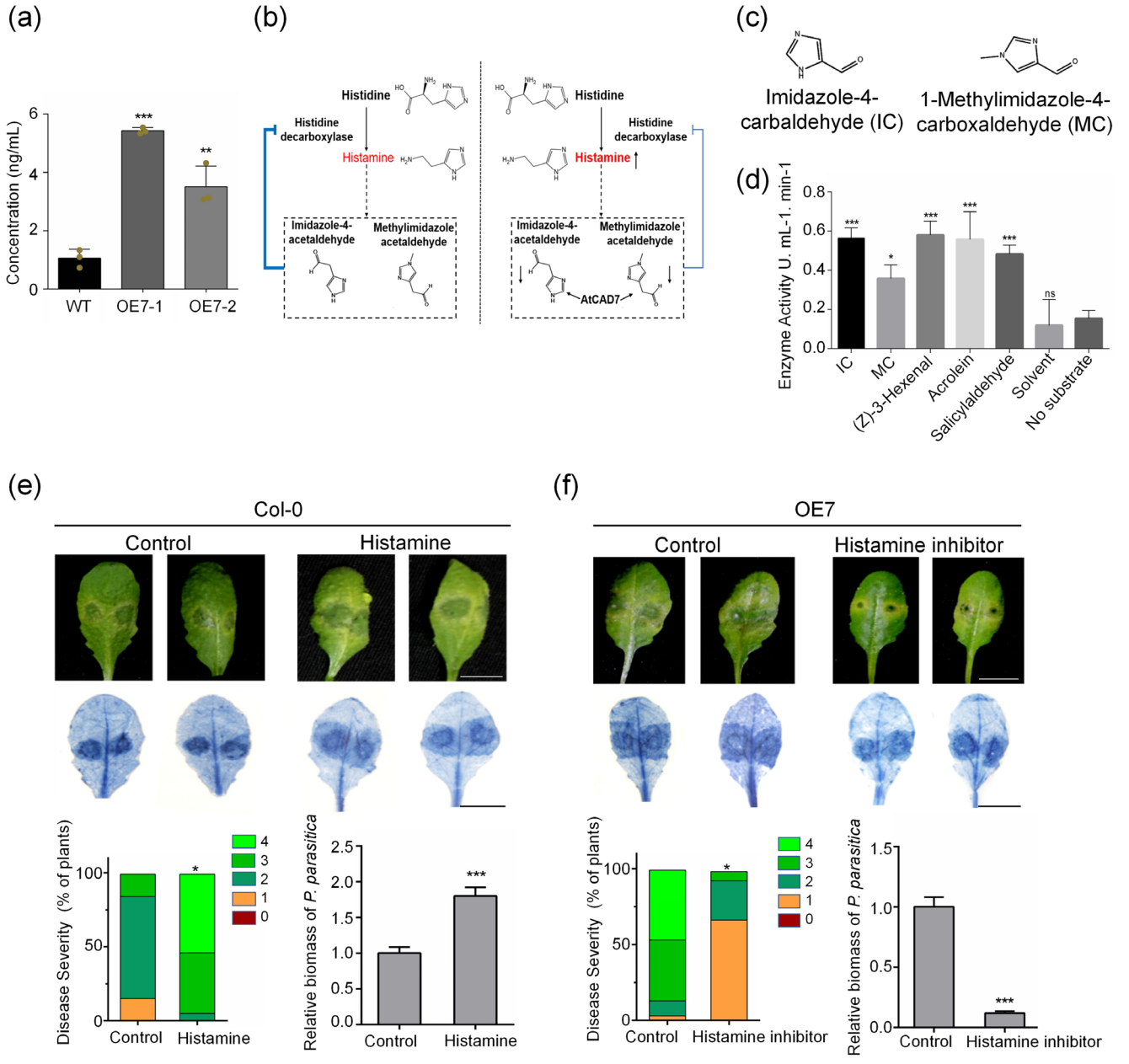

FIGURE 4 | Legend on next page.

FIGURE 4 | Overexpression of *AtCAD7* increased histamine accumulation and plant susceptibility to *Phytophthora parasitica*. (a) Total histamine contents in *Arabidopsis thaliana* wild type (WT) and the *AtCAD7*-overexpression lines OE7-1 and OE7-2 by LC–MS/MS. Values are presented as mean ± SD (Student's *t* test, $n = 3$, $^{**}p < 0.01$, $^{***}p < 0.001$). (b) Catabolic pathway of histamine biosynthesis in plants mediated by small molecule aldehyde reductase CAD7. Histamine-derived aldehydes decrease HDC protein concentration and thus reduce its activity. *AtCAD7* overexpression increased catalysis of histamine-derived aldehydes, leading to attenuated inhibition of histamine-derived aldehydes on HDC and increased histamine levels. (c) Chemical structures of imidazole-4-carbaldehyde and 1-methylimidazole-4-carboxaldehyde, which are structurally similar to the key metabolites in the histamine catabolic pathway. (d) Small-molecule aldehyde reductase activity of CAD7 toward imidazole-4-carbaldehyde and 1-methylimidazole-4-carboxaldehyde. The enzymatic activity of recombinant AtCAD7 was quantitatively analysed by spectrophotometry using imidazole-4-carbaldehyde (IC), 1-methylimidazole-4-carboxaldehyde (MC), and reference substrates including (*Z*)-3-hexenal, acrolein and salicylaldehyde. Two negative controls, solvent (substrate solvent) and no substrate, were included. Purified AtCAD7 protein was used, and catalytic rates were measured under standardised reaction conditions. Data represent the mean ± SD of triplicate biological replicates. Statistical significance was assessed by Student's *t* test ($^{*}p < 0.05$, $^{***}p < 0.001$, ns, not significant). (e) Exogenous histamine treatment increased *A. thaliana* susceptibility to *P. parasitica*. The leaves of 4-week-old wild-type Col-0 seedlings were treated with 20 μM histamine, with water as mock treatment, followed by inoculation with *P. parasitica* zoospores (~2000). Images were taken at 72 h post-inoculation (hpi). The leaves were stained by trypan blue to show the lesions. The statistical significance was assessed by the Wilcoxon–Mann–Whitney test. Similar results were observed in three independent experiments. The biomass of *P. parasitica* is shown as the mean ± SD of three repeats. Statistical significance was assessed by Student's *t* test for biomass analysis ($^{*}p < 0.05$, $^{***}p < 0.001$). Scale bars, 1 cm. (f) Exogenous treatment with histamine biosynthesis inhibitor reduced *A. thaliana AtCAD7*-overexpression lines OE7 susceptibility to *P. parasitica*. The leaves of 4-week-old wild-type Col-0 seedlings were treated with 40 μM histamine biosynthesis inhibitors, with water as mock treatment, followed by inoculation with *P. parasitica* zoospores (~2000). Images were taken at 72 hpi. The leaves were stained by trypan blue to show the lesions. The statistical significance was assessed by Wilcoxon–Mann–Whitney test. Similar results were observed in three independent experiments. Biomass of *P. parasitica* is shown as the mean ± SD of three repeats. Statistical significance was assessed by Student's *t* test for biomass analysis ($^{*}p < 0.05$, $^{***}p < 0.001$). Scale bars, 1 cm.

showed increased *P. parasitica* colonisation in histamine-treated leaves compared to that of the mock control (Figure 4e). The enhanced susceptibility induced by histamine treatment is consistent with the results showing promoted plant susceptibility by *CAD7* overexpression (Li et al. 2019). Meanwhile, after overexpressing *GFP-NbHDC* in *N. benthamiana*, quantitative detection via LC–MS/MS showed that the histamine levels were significantly higher than that in the *FLAG-GFP* control (Figure S6b). Infection assay showed that overexpression of *GFP-NbHDC* resulted in enhanced plant susceptibility to *P. parasitica* compared with the negative control *FLAG-GFP* (Figure S6c). The expression and integration of GFP-NbHDC and FLAG-GFP proteins were confirmed by western blotting (Figure S6d).

The histamine biosynthesis inhibitor 4-bromo-3-hydroxybenzoic acid (BHOA) inhibits histamine decarboxylase, leading to suppressed histamine levels (Qian et al. 2019). We examined histamine accumulation in OE7 plants treated with histamine biosynthesis inhibitor. Quantification via LC–MS/MS method confirmed that treatment with the inhibitor significantly reduced histamine accumulation in OE7 lines (Figure S6e). Leaves of OE7 lines exogenously treated with this histamine biosynthesis inhibitor exhibited enhanced resistance to *P. parasitica* compared to the mock controls. Furthermore, pathogen biomass quantification consistently revealed decreased levels of *P. parasitica* colonisation in inhibitor-treated OE7 leaves compared to that in the mock controls (Figure 4f), suggesting that attenuated histamine levels could reduce plant susceptibility mediated by *AtCAD7* overexpression to *P. parasitica*. These results indicate that histamine enhances plant susceptibility to the infection of *P. parasitica*, and histamine might be one of the key factors for *AtCAD7*-mediated plant susceptibility.

We further analysed whether histamine has a direct effect on *P. parasitica* growth, as well as its effect on plant susceptibility. Mycelial growth was not affected when cultured on a medium containing 20 μM histamine (Figure S7a), and *P. parasitica* did not show any notable morphological changes (Figure S7b), indicating that histamine does not affect pathogen growth, but more likely affects plant immunity to *P. parasitica*.

2.5 | *AtCAD7*-Silencing Lines Show Increased Accumulation of Scopolin and Chlorogenic Acid and Enhanced Resistance to *P. parasitica*

Metabolic profiling revealed upregulated metabolites in Ri7 lines and identified two candidate phytoalexins, scopolin and chlorogenic acid. Consistent with the results of metabolomic analysis, LC–MS/MS analysis showed that the contents of scopolin and chlorogenic acid in *AtCAD7*-silencing (Ri7) lines were 2 and 4 times higher than those in the WT, respectively (Figure 5a). In vitro assays demonstrated their suppressing activities against *P. parasitica* growth. When cultured in a medium containing 20 μM scopolin and chlorogenic acid, mycelial growth was significantly reduced compared with the mock control (Figure S7a). *P. parasitica* hyphae exhibited severe morphological alterations, including shortened length and excessive branching, which are indicative of growth inhibition (Figure S7b). Exogenous application of 20 μM scopolin and chlorogenic acid to *A. thaliana* leaves via petiole infiltration, followed by *P. parasitica* inoculation, showed their restrictive effect on lesion development compared to the mock controls (Figure 5b,c). Quantification of *P. parasitica* biomass consistently confirmed their immune role in suppressing pathogen infection (Figure 5b,c). These results suggest that scopolin and chlorogenic acid promote *A. thaliana* resistance to *P. parasitica* infection.

Phenylalanine ammonia-lyase 1 (*PAL1*), *p-coumaroylshikimate/quinate 3′-hydroxylase* (*C3′H*) and *feruloyl-CoA 6′-hydroxylase 1* (*F6′H1*) are key genes encoding components of the phenylpropanoid pathway, playing important roles in regulating accumulation of chlorogenic acid and scopolin in *A. thaliana* and other

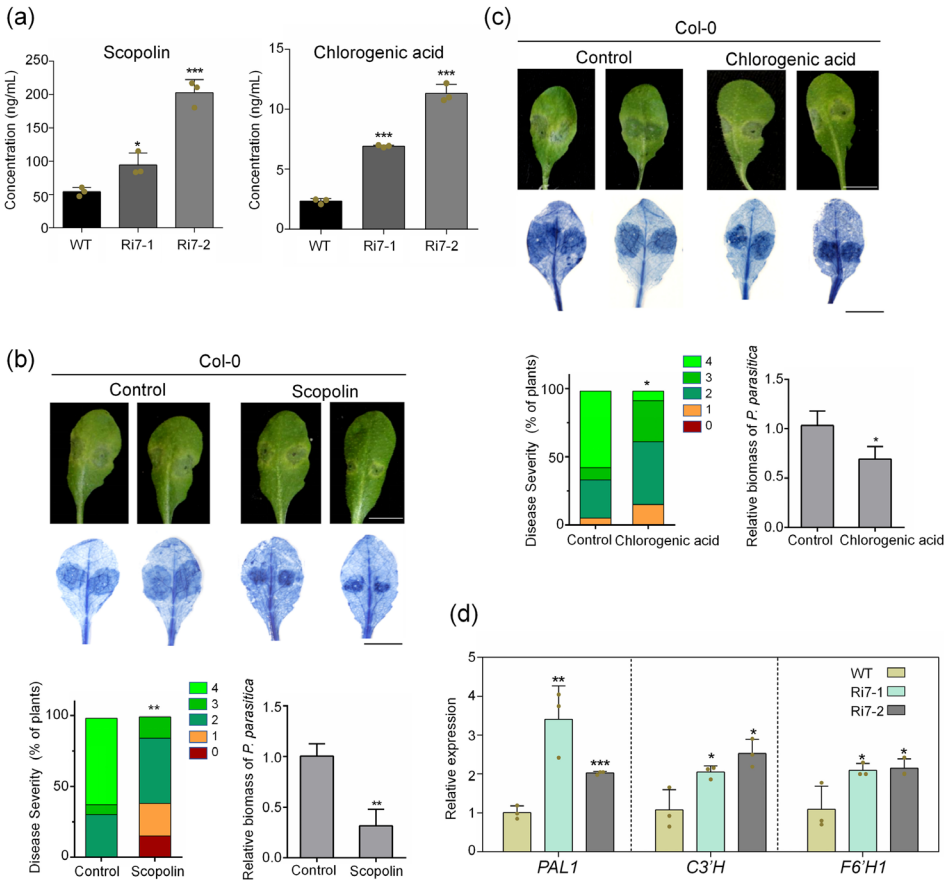

FIGURE 5 | Exogenous treatment with scopolin and chlorogenic acid enhanced plant resistance to *Phytophthora parasitica*. (a) Total scopolin and chlorogenic acid contents in wild type (WT) and the *AtCAD7*-silenced lines Ri7-1 and Ri7-2 by LC–MS/MS. Values are presented as mean ± SD (Student's *t* test, $n = 3$, $^{*}p < 0.05$, $^{***}p < 0.001$). (b, c) Exogenous treatment with scopolin (b) and chlorogenic acid (c) enhanced *Arabidopsis thaliana* resistance to *P. parasitica*. The leaves of 4-week-old WT Col-0 seedlings were treated with 20 μM scopolin and chlorogenic acid, with water as a mock treatment, followed by inoculation with *P. parasitica* zoospores (~2000). Images were taken at 72 h post-inoculation for the assessment of disease severity of the infected leaves. The leaves were stained by trypan blue to show the lesions. The statistical significance was assessed by Wilcoxon–Mann–Whitney test. Similar results were observed in three independent experiments. Biomass of *P. parasitica* is shown as the mean ± SD of three repeats. Statistical significance was assessed by Student's *t* test for biomass analysis ($^{*}p < 0.05$, $^{**}p < 0.01$). Scale bars, 1 cm. (d) Reverse transcription-quantitative PCR results showing the expression levels of phenylpropanoid-related genes (*PAL1*, *C3′H*, and *F6′H1*) in the WT and *AtCAD7*-silenced lines Ri7-1 and Ri7-2. Results are presented as the mean ± SD of at least three repeats. Statistical significance was assessed by Student's *t* test. $^{*}p < 0.05$, $^{**}p < 0.01$, and $^{***}p < 0.001$.

plants (Soviguidi et al. 2021; He et al. 2022). They exert critical functions in plant immunity (Beesley et al. 2023; Li et al. 2022). As shown in Figure S8, *P. parasitica* infection significantly up-regulated transcript levels of *PAL1*, *C3′H* and *F6′H1* in *A. thaliana*, with steady transcript increases over infection time points. Our comparative analysis revealed that the transcript levels of *PAL1*, *C3′H* and *F6′H1* in Ri7 lines were higher than those in the WT plants (Figure 5d), suggesting that *AtCAD7*-silenced lines are activated in the expression of *PAL1*, *C3′H* and *F6′H1*, and are consequently increased with accumulation of chlorogenic acid and scopolin, and enhanced plant resistance to *P. parasitica*.

3 | Discussion

AtCAD7 has emerged as an enzyme with distinct substrates from lignin biosynthesis and expanding roles in plant defence (Li et al. 2019; Tanaka et al. 2018). It has distinct catalytic specificity toward small-molecule aldehydes, differing from classical lignin-related cinnamyl alcohol dehydrogenase members such as AtCAD4 and AtCAD5. Cinnamyl alcohol dehydrogenases are NADPH-dependent oxidoreductases belonging to the medium-chain dehydrogenase/reductase (MDR) superfamily (Kim et al. 2004). Enzymes in this family can catalyse both dehydrogenation (oxidising alcohols to aldehydes/ketones) and reduction (converting aldehydes/ketones to alcohols) (Jörnvall 2008). Our study reveals that AtCAD7 specifically reduces diverse small-molecule aldehydes through an NADPH-dependent catalytic reaction, aligning its function more closely with that of a small-molecule aldehyde reductase. This is analogous to the designation of AtCAD7 as hexenal reductase by Tanaka et al. (2018) based on its ability to catalyse hexenal. AtCAD8 is more specific for aromatic aldehydes (Somssich et al. 1996), whereas our results indicate that AtCAD7 exhibits broader substrate specificity, including aliphatic aldehydes and aromatic aldehydes.

Structural analyses further indicated that AtCAD7 shares conserved catalytic residues with *E. coli* alcohol dehydrogenases

EcYahK and EcYjgB (Figure 1b), while differences in key active site residues endow it with broader substrate selectivity. Our comparative enzymatic assays with AtCAD5 further validated this functional divergence, with AtCAD5 exhibiting a high level of activity toward *p*-coumaryl aldehyde (a lignin precursor) and AtCAD7 negligible activity toward this substrate but efficient catalytic activity toward small-molecule aldehydes (Figure S4), including histamine-derived intermediates (1-methylimidazole-4-carboxaldehyde and imidazole-4-carbaldehyde). This is consistent with sequence alignments showing that AtCAD7 shares conserved catalytic residues with EcYahK and EcYjgB rather than canonical CADs. This evolutionary convergence suggests its functional diversification, playing a role as a versatile aldehyde reductase, which enables its participation in metabolic pathways beyond lignin biosynthesis. For instance, previous studies have demonstrated that AtCAD7 is involved in GLV metabolism (Tanaka et al. 2018). It can convert (*Z*)-3-hexenal to (*Z*)-3-hexen-1-ol during wound-induced GLV bursts, fine-tuning the balance between toxic aldehydes and predator-attracting alcohols to optimise indirect herbivore defence. Thus, AtCAD7 bridges roles in pathogen response, herbivore deterrence and volatile signalling, exemplifying its metabolic plasticity in plant stress adaptation.

The AtCAD7 enzymatic activity likely disrupts the equilibrium of histamine catabolism, leading to an accumulation of histamine through feedback regulation. Histidine decarboxylase (HDC), the rate-limiting enzyme in histamine biosynthesis, catalyses the conversion of histidine to histamine (Huang et al. 2018). Its activity and expression are regulated by many factors such as substrates, products and inhibitors (Kelley et al. 1977; Kollonitsch et al. 1978; Moriguchi and Takai 2020; Qian et al. 2019; Wu et al. 2008). Specifically, the depletion of aldehyde intermediates may relieve feedback inhibition on HDC, thereby upregulating histamine production (Figure 4b) (Li et al. 2024; Naz et al. 2023). To confirm the feedback regulation mechanism, we showed that histamine-derived aldehydes (1-methylimidazole-4-carboxaldehyde and imidazole-4-carbaldehyde) decreased NbHDC protein levels in planta (Figure S6a), indicating their activity to reduce HDC levels, as quantified by using a plant histidine decarboxylase ELISA detection kit. Furthermore, transient overexpression of *NbHDC* in *N. benthamiana* increased histamine levels, as detected via LC–MS/MS, and enhanced plant susceptibility to *P. parasitica* (Figure S6).

We found that leaves of the *AtCAD7*-overexpressing lines exogenously treated with a histamine biosynthesis inhibitor, BHOA, exhibited enhanced resistance to *P. parasitica*. No previous reports have documented the application of histamine biosynthesis inhibitors in plants; we hypothesise that this inhibitor is applicable to suppression of histamine synthesis in plants. Its mechanism of action involves specific targeting to HDC, a rate-limiting enzyme in histamine biosynthesis, by competing for its active site and interfering with the interaction between HDC and its cofactor pyridoxal-phosphate (PLP), thereby impairing enzymatic activity and inhibiting histamine synthesis (Levine and Noll 1969; Moya-García et al. 2009; Qian et al. 2019). The rationale for this cross-species applicability lies in the conserved histamine biosynthetic pathway between animals and plants. Histamine is generated via the decarboxylation of L-histidine catalysed by PLP-dependent HDC in both systems (Facchini et al. 2000; Kumar 2016). Furthermore, histamine accumulation in OE7 lines following treatment with BHOA showed significant reduction (Figure S6e). However, potential risks may exist in plants, including unintended effects on other PLP-dependent enzymes (e.g., aromatic L-amino acid decarboxylase involved in defence metabolite biosynthesis and glutamate decarboxylase regulating stress resistance) (Facchini et al. 2000; Kumar 2016). BHOA is a derivative of benzoic acids (BAs), which are released by plants through leaching of leaf exudates and rhizodeposition, and most of them exert allelopathic effects and influence numerous physiological processes (Maffei et al. 1999; Zhang et al. 2025). Studies have shown that hydroxy-substituted BAs, such as *m*-hydroxybenzoic acid (*m*HB), which shares structural similarity with BHOA, can promote cucumber seed germination, seedling biomass and isocitrate lyase (ICL) activity at appropriate concentrations (0.1–1 mM) (Maffei et al. 1999). The concentration ranges of 0.1–1 mM is the bioactive range for most phenolic compounds (Maffei et al. 1999). Therefore, we hypothesise that the use of BHOA at low concentrations (0.04 mM) is non-toxic to plants.

Histamine was shown to activate *Pseudomonas aeruginosa* transcription factors and genes associated with its pathogenicity, thereby enhancing its virulence (Krell et al. 2021; Wang et al. 2021). Although the role of histamine in animal–pathogen interactions has been well-characterised, its involvement in plant–microbe interaction remains underexplored. Histamine accumulation increases production of downstream metabolites like imidazole-4-acetic acid (ImAA). In bacteria, ImAA directly binds to and activates the transcriptional regulator HinK, enhancing its affinity for target DNA and inducing the expression

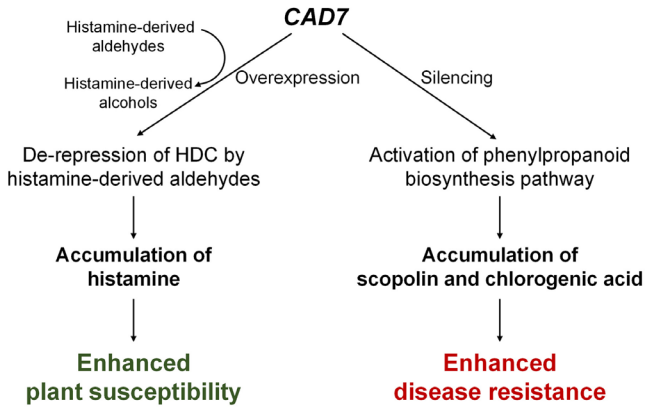

FIGURE 6 | Proposed model of AtCAD7 function. As a small-molecule aldehyde reductase, AtCAD7 catalyses the conversion of diverse small aldehyde substrates, including histamine-derived aldehydes. In *AtCAD7*-overexpression lines, the small-molecule aldehyde reductase activity of AtCAD7 uses NADPH as a coenzyme factor to reduce imidazole-4-carbaldehyde and 1-methylimidazole-4-carboxaldehyde to their corresponding alcohols. This achieves the derepression of histamine-derived aldehydes on histidine decarboxylase (HDC), thereby enhancing histamine accumulation and plant susceptibility to *Phytophthora parasitica*. In *AtCAD7*-silenced lines, the content of scopolin and chlorogenic acid is increased through the activated phenylpropanoid biosynthetic pathway, resulting in enhanced plant disease resistance.

of virulence-related genes that promote pathogen adaptability and virulence in the host environment (Wang et al. 2021). Our study provides the first empirical evidence of the function of histamine in plant–oomycete interactions. In *AtCAD7*-overexpressing lines, AtCAD7, as a small-molecule aldehyde reductase, catalyses the conversion of histamine-derived aldehydes, thereby reducing the feedback inhibition of histidine decarboxylase, in turn increasing histamine levels and enhancing plant susceptibility to *P. parasitica* (Figure 6). However, whether this mechanism is applicable to other pathogens requires further investigation, which forms part of future research. Additionally, the specific mechanisms by which *Phytophthora* utilises histamine and histamine enhances plant susceptibility to *P. parasitica* await further elucidation.

The silencing of *AtCAD7* in Ri7 lines led to a marked accumulation of defence-related secondary metabolites, including flavonoids, phenolic acids, tannins and lipids (Figure 3a). These compounds are known for their roles in plant–pathogen interactions and collectively establish a multilayered defence system against microbial invasion (Jones et al. 2024). The flavonoids with relatively higher accumulation in Ri7 lines include phloretin-2′-*O*-glucoside (phlorizin), quercetin-7-*O*-glucoside, and 6-hydroxykaempferol-7,6-*O*-diglucoside. These compounds disrupt pathogen membrane integrity via oxidative stress induction (Kai et al. 2021) and interfere with pathogen effector secretion (Ziani et al. 2018). We found phenolic acid compounds, including 5-*O*-caffeoylquinic acid, chlorogenic acid and coniferin, in Ri7 lines. The 5-*O*-caffeoylquinic acid is a natural antibacterial substance that can be used against pathogenic microorganisms (Ziani et al. 2018). Chlorogenic acid is a plant polyphenol with antioxidant and bacteriostatic activities and can inhibit the postharvest rot of cherry tomato fruit caused by *Fusarium fujikuroi* by inducing cellular oxidative stress in the pathogen (Kai et al. 2021). High concentrations of coniferin contribute to defence responses against *Verticillium longisporum* (König et al. 2014). Scopolin accumulated in Ri7 lines (Figures 3a and 5a) and is present in many plants (Gnonlonfin et al. 2012). It has antibacterial, bactericidal and insecticidal properties (Beyer et al. 2019; Prats et al. 2006; Stringlis et al. 2018). It selectively inhibits fungal pathogens in soil, promotes beneficial plant rhizosphere bacteria, and induces systemic resistance responses to root diseases (Stringlis et al. 2018). As the key initiating gene in the phenylpropanoid pathway, *PAL1*, together with *C3′H* and *F6′H1* that serve as key genes in this pathway, enhances plant resistance to pathogens by initiating the biosynthesis of immunity-related secondary metabolites such as lignin and flavonoids. The level of their expression directly affects the disease resistance of plants (Beesley et al. 2023; Li et al. 2022; Ninkuu et al. 2025; Vanholme et al. 2019). The accumulation of scopolin and chlorogenic acid in Ri7 lines was accompanied by upregulated transcription of *PAL1*, *C3′H* and *F6′H1*. This transcriptional activation supports the notion that *AtCAD7*-silencing specifically activates the phenylpropanoid pathway, leading to increased synthesis of these defence metabolites (Figure 6). Nevertheless, the plant immune system is a complex, multilayered physiological process, and the strength of plant disease resistance is determined by multiple factors, including the efficiency of plant immune signal transduction and the expression levels of disease resistance genes (Liu et al. 2025; Ngou et al. 2022; Tang et al. 2025; Wang et al. 2025). Furthermore, pathogen effectors are well-documented to modulate plant disease resistance by interfering with the plant immune system (Liu et al. 2025; Ngou et al. 2022; Tang et al. 2025; Wang et al. 2025). Thus, how the silencing of *AtCAD7* specifically activates plant defence requires further investigation.

Metabolomic analysis indicated several clear differences in metabolite accumulation in the tested lines. We detected histamine in the up-regulated metabolites of OE7 and found that it could promote plant susceptibility to *Phytophthora* infection. We also detected disease-resistant metabolites in the up-regulated metabolites of Ri7, in which scopolin and chlorogenic acid could effectively inhibit *Phytophthora* infection. Unravelling such mechanisms not only deepens our understanding of plant–pathogen interactions but also provides actionable targets for sustainable crop improvement.

4 | Experimental Procedures

4.1 | Plant Materials

The wild-type *A. thaliana* used in this study was Col-0. The three independent AtCAD7-overexpressing (OE7-1, OE7-2, OE7-3) and two independent AtCAD7-silenced (Ri7-1, Ri7-2) lines were generated via *Agrobacterium tumefaciens*-mediated transformation of wild-type Col-0 plants, as described (Li et al. 2019). All *A. thaliana* plants used in this study were grown at 23°C with 14 h of light per 24 h.

4.2 | Plasmid Construction

The full-length coding sequences of *AtCAD7* (AT4G37980) and *AtCAD5*(AT4G34230) were amplified from *A. thaliana* Col-0 cDNA. *NbHDC* (Niben101Scf01777g00016.1) was amplified from cDNA generated from *N. benthamiana* leaves. For in vitro assays, *AtCAD7*, *AtCAD5, EcYahK* (NP_414859.1) and *EcYjgB* (CAQ34616.1) sequences were cloned into the pET32a vector using NcoI and XhoI restriction sites to encode thioredoxin+histidine-tagged Trx-His-AtCAD7, Trx-His-AtCAD5, Trx-His-EcYahK, and Trx-His-EcYjgB. The *NbHDC* sequence was fused to sequences encoding green fluorescent protein (GFP) by cloning into the pART27-N vector using EcoRI and XbaI sites to create constructs encoding GFP-NbHDC fusion proteins. All primers used for plasmid constructions are listed in Table S3.

4.3 | Chemicals and Reagents

NADH and NADPH were purchased from MedChemExpress. (*Z*)-3-hexenal, acrolein, methylbutanal, isovaleraldehyde, benzaldehyde, 2-methoxybenzaldehyde, 3-methoxybenzaldehyde, salicylaldehyde, *p*-coumaryl aldehyde and 2-methoxyethanol were purchased from Aladdin. LC–MS grade methanol, formic acid, and acetonitrile were purchased from Fisher Scientific. All other chemicals used were of analytical grade or higher.

4.4 | Pathogen Culture Condition and Infection Assays

Oomycete pathogen *P. parasitica* isolate Pp016 was used for *A. thaliana* infection assays. *P. parasitica* was grown on CA medium with 5% (vol/vol) carrot juice, 0.01% (wt/vol) $CaCO_3$ and 0.005% (wt/vol) β-sitosterol. Detached leaves of approximately 4-week-old *A. thaliana* were injected with distilled water or histamine solution (20 μM) or histamine biosynthesis inhibitor (40 μM) or scopolin solution (20 μM) or chlorogenic acid solution (20 μM) and incubated at 23°C with a photoperiod of 13 h light and 11 h dark for 24 h. The remaining chemical solution on the leaves' surface was removed and then leaves were inoculated with *P. parasitica* zoospores at 23°C for 3 days post-inoculation (dpi). For the detached leaf inoculation assay, the petioles of detached plant leaves were wrapped with moist cotton, and the leaves were placed on moist filter paper in a plastic tray and a *P. parasitica* zoospore suspension of the appropriate concentration was applied as droplets to the abaxial side of the leaf. Plant leaves were drop-inoculated with 2000 zoospores for *P. parasitica*. *A. thaliana* leaves with infection were categorised into five grades: Grade 1, minimal infection; Grade 2, lesion radius less than 1/4 of the leaf radius; Grade 3, lesion radius ranging from 1/4 to 1/2 of the leaf radius; Grade 4, lesion radius between more than 1/2 and 3/4 of the leaf radius; Grade 5, complete leaf infection. The lesion sizes and pathogen biomass were used to evaluate the plant disease severity. The genomic DNA was extracted using the cetyltrimethylammonium bromide (CTAB) method, and the RT-qPCR assays were used to determine the pathogen biomass. Eight leaves were used for each experiment, and three biological replicates were performed.

4.5 | Production of Recombinant Proteins in *E. coli*

pET32a-*AtCAD7*, pET32a-*AtCAD5*, pET32a-*EcYahK*, and pET32a-*EcYjgB* constructs were transformed into *E. coli* BL21 (DE3). Transformed *E. coli* cells harbouring respectively the *AtCAD7*, *AtCAD5*, *EcYahK*, and *EcYjgB* constructs were cultured in Luria Bertani (LB) medium supplemented with 50 μg/mL ampicillin at 37°C. Protein expression was induced by adding 0.5 mM isopropyl-β-D-thiogalactopyranoside (IPTG) until an OD_{600} of 0.6–0.8 was reached. The culture was subsequently incubated at 18°C for 16 h to facilitate recombinant protein synthesis. Cells were harvested by centrifugation at 6000 *g* for 10 min at 4°C, washed twice with ice-cold Tris–HCl buffer, and resuspended in 20 mM Tris–HCl buffer (pH 8.0) containing 300 mM NaCl and 5 mM imidazole. Cell lysis was performed using an ultrasonic cell crusher (Ningbo Scientz Biotechnology). The lysate was clarified by centrifugation at 12,000 *g* for 30 min at 4°C, and the supernatant containing soluble proteins was collected as crude extract. Recombinant AtCAD7, AtCAD5, EcYahK and EcYjgB proteins were purified by immobilised metal affinity chromatography using a Ni NTA Beads 6FF agarose column (Smart-Life Sciences). The column was equilibrated with 5 mM imidazole, and bound proteins were eluted with 250 mM imidazole in the same buffer. Eluted fractions were analysed by 10% SDS-PAGE and visualised by Coomassie brilliant blue staining.

4.6 | Enzymatic Assays

The catalytic activity of AtCAD7, AtCAD5, EcYahK and EcYjgB proteins were determined spectrophotometrically by monitoring NADPH oxidation at 340 nm, where absorbance decreases proportionally to coenzyme consumption during aldehyde reduction. Reaction mixtures (1 mL) contained 50 μg purified proteinase in 50 mM potassium phosphate buffer (pH 6.5). Substrates ((*Z*)-3-hexenal, acrolein, methylbutanal, isovaleraldehyde, benzaldehyde, 2-methoxybenzaldehyde, 3-methoxybenzaldehyde, salicylaldehyde, *p*-coumaryl aldehyde) were dissolved in 2-methoxyethanol at 100 mM stock concentrations, with 1 μL added to achieve 100 μM final concentration. Reactions were initiated by adding 10 μL of a 20 mM NADPH stock solution to achieve a final concentration of 200 μM after a 5 min pre-incubation at 30°C. Four types of negative controls were included to account for non-enzymatic reactions and background signals: (1) substrate solvent control, reaction mixture containing 50 μg purified AtCAD7, 50 mM potassium phosphate buffer (pH 6.5), 200 μM NADPH, and 1 μL 2-methoxyethanol; (2) no-enzyme control, reaction mixture containing 50 mM potassium phosphate buffer (pH 6.5), 200 μM NADPH, and 1 μL substrate (100 μM acrolein, (*Z*)-3-hexenal, salicylaldehyde); (3) heat-inactivated enzyme control, reaction mixture with 50 μg purified AtCAD7 treated at 90°C for 10 min (to eliminate catalytic activity), plus 50 mM potassium phosphate buffer (pH 6.5), 200 μM NADPH, and 1 μL substrate (100 μM acrolein, (*Z*)-3-hexenal, salicylaldehyde); (4) no-substrate control, reaction mixture containing 50 μg purified AtCAD7, 50 mM potassium phosphate buffer (pH 6.5), 200 μM NADPH. A blank control consisting of only 50 mM potassium phosphate buffer (pH 6.5) and 1 μL 2-methoxyethanol (no enzyme, no substrate, no NADPH) was also prepared for background correction. Absorbance kinetics were recorded immediately at 340 nm using a microplate reader (Thermo Fisher Scientific) equipped with temperature-controlled cuvette holders. For background correction, the measured change in absorbance of the complete reaction system (with purified proteinase, substrate and NADPH) is subtracted by the change in absorbance of the blank control (containing only buffer, 2-methoxyethanol and NADPH) to calculate the actual enzyme activity. Substrate specificity profiles were generated by comparing initial reaction velocities (ΔA_{340}/min) across tested aldehydes, normalised to protein concentration.

For detection of plant histidine decarboxylase, a plant histidine decarboxylase kit was used (MEIMIAN). This kit employs double antibody one-step sandwich ELISA. Samples, standards and horseradish peroxidase (HRP)-labelled detection antibody were sequentially added into coated microplates precoated with histidine decarboxylase HDC antibody, followed by incubation and thorough washing. The reaction (colour development) was done with substrate TMB, which converts to blue under catalysis of peroxidase and to final yellow under action of acid. Intensity is positively correlated with quantity of histidine decarboxylase HDC in samples. Absorbance at 450 nm wavelength was measured using a microplate reader and sample concentrations were calculated, and a standard curve was generated based on the standards. Standard concentrations were as follows: 0, 15, 30, 60, 120, 240 ng/mL. Two negative controls were included,

infiltration of substrate solvent 2-methoxyethanol 2 days after overexpression of *NbHDC* or *FLAG-GFP* for the experimental group, infiltration of imidazole-4-carbaldehyde and 1-methylim idazole-4-carboxaldehyde was performed separately 2 days after overexpression of *NbHDC*. Absorbance was measured at 450 nm using a microplate reader, and sample concentrations were calculated based on the standard curve.

4.7 | Thin-Layer Chromatography

Thin-layer chromatography (TLC) was used to detect the formation of enzymatic reaction products. The enzymatic reaction was carried out at 30°C in a volume of 1 μL for 30 min. The reaction system contained 200 mM potassium phosphate buffer and NADPH. Two representative substrates, 5 mM salicylaldehyde and 2-methoxybenzaldehyde, along with 50 μg of CAD7 protein, were selected. In a saturated chamber, 5 μL of each enzymatic reaction mixture and standard were spotted onto a silica gel plate using chloroform as the eluent. The chromatograms were directly observed under ultraviolet light at 254 nm.

4.8 | Metabolite Extraction and Analysis

Metabolite profiling was performed on three independent *AtCAD7*-overexpression lines (OE7-1, OE7-2, OE7-3) and two independent *AtCAD7*-silenced lines (Ri7-1, Ri7-2) generated as described (Li et al. 2019), along with WT Col-0 plants. For each genotype, three biological replicates were analysed, each consisting of pooled leaf tissues from 10 individual plants per independent line. About 100 mg of the powder were suspended in 1.2 mL of 70% methanol by vortexing six times, followed by incubation at 4°C overnight. The solution was then centrifuged at 12,000 *g* for 10 min, and the supernatant was aspirated for UPLC–MS/MS analysis. The main data acquisition instrumentation systems were ultra performance liquid chromatography (UPLC) and tandem mass spectrometry (MS/MS). The chromatographic columns used were Agilent SB-C18 1.8 μm, and 2.1 × 100 mm. The mobile phase conditions were as follows: phase A was double-distilled water (with 0.1% formic acid added), and phase B was acetonitrile (with 0.1% formic acid added). The flow rate was 0.35 mL/min, the column temperature was 40°C, and the injection volume was 4 μL. After separating small molecules by UPLC, we used Analyst v. 1.6.3 on MS/MS to run both positive and negative ionisation modes. Metabolite quantification was accomplished using multiple reaction monitoring (MRM) analysis. The data were processed using the software Analyst v. 1.6.3 and MultiaQuant. Significantly regulated metabolites between groups were determined by VIP ≧ 1 and absolute $\log_2$ fold change ≧ 1. VIP values were extracted from the OPLS-DA result. Identified metabolites were annotated using the KEGG compound database (http://www.kegg.jp/kegg/compound/), and annotated metabolites were then mapped to the KEGG pathway database (http://www.kegg.jp/kegg/pathway.html). The rich factor is defined as the ratio of the number of differentially expressed metabolites in the corresponding pathway to the total number of metabolites annotated in the pathway detection. Larger values indicate a greater degree of enrichment. Pathway analysis of differential metabolites was carried out on significantly different known metabolites using the pathway library of *A. thaliana* (Hawkins et al. 2025).

4.9 | Transient Expression in *N. benthamiana*

Agrobacterium tumefaciens GV3101 cells transformed with each construct were grown in LB broth with appropriate antibiotics at 28°C overnight. Cells were resuspended in infiltration buffer (10 mM 2-(*N*-morpholino)-ethanesulfonic acid, 10 mM $MgCl_2$, 200 μM acetosyringone) to an OD_{600} of 0.2–0.5, then incubated at room temperature for 1 h prior to infiltration experiments. Following transient expression in *N. benthamiana* for 2 days, appropriate assays were performed.

4.10 | Extraction and Quantification of Histamine Scopolin and Chlorogenic Acid

Histamine extraction and quantification were conducted as previously described (Zhang et al. 2021) with minor modifications. Briefly, 1 g of frozen leaf samples was extracted with 1 mL of extraction buffer and incubated overnight at 4°C. The samples were then centrifuged at 12,000 *g* for 20 min at 4°C. The supernatants were collected, and the pellets were re-extracted twice each with 0.5 mL of extraction buffer. Combined supernatants yielded a final volume of 2 mL. Samples were filtered through a 0.22 μm filter and analysed for metabolites using a liquid chromatography mass spectrometry (LC-MS) system (SCIEX QTRAP5500) equipped with an ACQUITY HSS T3 column (2.1 × 100 mm, 1.8 μm, Waters) at a flow rate of 0.3 mL/min. The solvent system consisted of water (A) containing 0.1% (vol/vol) formic acid and acetonitrile (B). The linear gradient programme was set as follows: 2% B from 0 to 1 min, linear increase from 0% to 50% B from 1 to 5 min, linear increase from 50% to 98% B from 5 to 6.5 min, linear decrease from 98% to 2% B from 7.5 to 8 min, and 2% to 0% B from 8 to 13 min. The automatic injector temperature was maintained at 15°C. MS analysis of histamine was performed in multiple reaction monitoring (MRM) mode with electrospray ionisation in positive ion mode. Data quantification was achieved by comparing sample peak areas with those obtained from standard histamine (Sigma). Histamine standards were diluted with extraction buffer to form the following concentration range: 0.1, 0.2, 0.5, 1, 5, 10, 50 ng/mL.

Scopolin and chlorogenic acid were extracted with 80% methanol. Samples were filtered through a 0.22 μm filter and analysed using an LC-MS system equipped with a Hypersil GOLD Dim column (2.1 × 100 mm × 3 μm, Thermo) at a flow rate of 0.3 mL/min. The solvent system comprised water (A) with 0.1% (vol/vol) formic acid and methanol (B). The elution gradient was set as follows: 5% B from 0 to 2 min, linear increase from 5% to 40% B from 2 to 10 min, linear increase from 40% to 95% B from 10 to 15 min, 95% B from 15 to 18 min, and linear decrease from 95% to 2% B from 18 to 20 min. The automatic injector temperature was 15°C. MS analysis of scopolin and chlorogenic acid was carried out in MRM mode with electrospray ionisation in negative ion mode. Quantification was performed by comparing sample peak areas with those of standard scopolin and chlorogenic acid, respectively. Scopolin and chlorogenic acid standards were each diluted with extraction buffer to generate the same

concentration range: 5, 20, 100, 500, 1000, 3500 ng/mL. The MRM conditions were *m/z* 112.2/68.0 for histamine, 353.0/148.9 for scopolin and 353.0/191.0 for chlorogenic acid, respectively.

4.11 | Gene Expression Analysis

Four-week-old leaves or 2-week-old roots of *A. thaliana* with inoculation or mock treatment were collected to extract total RNA using Total RNA Extraction Kit (TIANGEN) according to the manufacturer's instructions. cDNA was synthesised from the resulting RNA using PrimeScript RT reagent Kit with gDNA Eraser (TakaRa) for real-time quantitative PCR (qPCR). qPCR was performed on a LightCycler 480 Instrument (Roche Life Science) with the UltraSYBR Mix (CWBIO). Relative gene expression levels were calculated using the $2^{-\Delta\Delta Ct}$ method normalised with the reference genes *PpUBC9* for *P. parasitica* and *AtUBC9* for *A. thaliana*. Primers are listed in Table S3.

Author Contributions

Liwen Ding: writing – review and editing, writing – original draft, project administration, funding acquisition, resources. **Zewen Liu:** data curation, writing – original draft. **Weihang Wang:** methodology, data curation. **Yang Yang:** data curation, writing – review and editing. **Ren Sa:** methodology, data curation. **Hongmei Wang:** methodology, data curation. **Liru Mi:** data analysis. **Yalan Qin:** writing – review and editing. **Shaocong Kang:** methodology, data curation. **Meruyert Medelbek:** writing – review and editing. **Assiya Ansabayeva:** writing – review and editing. **Yuling Meng:** conceptualization, writing – review and editing. **Weixing Shan:** writing – review and editing, writing – original draft, project administration, funding acquisition, resources.

Acknowledgements

We thank Meijuan Ren (LSRCS, Northwest A&F University), Luqi Li (LSRCS, Northwest A&F University), Yao Liu (LSRCS, Northwest A&F University) and Yan Li (College of Plant Protection, Northwest A&F University) for technical support in LC–MS/MS, microplate reader and microscopy. This work was supported by the National Natural Science Foundation of China (#31930094), China Agriculture Research System (#CARS-09), and the State Administration of Foreign Experts Affairs (#B18042).

Funding

This work was supported by the National Natural Science Foundation of China, #31930094; China Agricultural Research System, #CARS-09; State Administration of Foreign Experts Affairs, #B18042.

Conflicts of Interest

The authors declare no conflicts of interest.

Data Availability Statement

The data that support the findings of this study are available from the corresponding author upon reasonable request.

References

Abraham, S. N., and R. Malaviya. 1997. "Mast Cells in Infection and Immunity." *Infection and Immunity* 65: 3501–3508.

Baker, S. A., and J. Rutter. 2023. "Metabolites as Signalling Molecules." *Nature Reviews Molecular Cell Biology* 24: 355–374.

Barakat, A., A. Bagniewska-Zadworna, A. Choi, et al. 2009. "The Cinnamyl Alcohol Dehydrogenase Gene Family in *Populus*: Phylogeny, Organization, and Expression." *BMC Plant Biology* 9: 26.

Barwell, L. J., A. Perez-Sierra, B. Henricot, A. Harris, and B. V. Purse. 2021. "Evolutionary Trait-Based Approaches for Predicting Future Global Impacts of Plant Pathogens in the Genus *Phytophthora*." *Journal of Applied Ecology* 58: 718–730.

Beesley, A., S. F. Beyer, V. Wanders, et al. 2023. "Engineered Coumarin Accumulation Reduces Mycotoxin-Induced Oxidative Stress and Disease Susceptibility." *Plant Biotechnology Journal* 21: 2490–2506.

Beyer, S. F., A. Beesley, P. F. W. Rohmann, H. Schultheiss, U. Conrath, and C. J. G. Langenbach. 2019. "The *Arabidopsis* Non-Host Defence-Associated Coumarin Scopoletin Protects Soybean From Asian Soybean Rust." *Plant Journal* 99: 397–413.

Bomati, E. K., and J. P. Noel. 2005. "Structural and Kinetic Basis for Substrate Selectivity in *Populus tremuloides* Sinapyl Alcohol Dehydrogenase." *Plant Cell* 17: 1598–1611.

Chen, J. Y., P. F. Wen, W. F. Kong, Q. H. Pan, S. B. Wan, and W. D. Huang. 2006. "Changes and Subcellular Localizations of the Enzymes Involved in Phenylpropanoid Metabolism During Grape Berry Development." *Journal of Plant Physiology* 163: 115–127.

Chonmaitree, T., J. A. Patel, M. A. Lett-Brown, et al. 1994. "Virus and Bacteria Enhance Histamine Production in Middle Ear Fluids of Children With Acute Otitis Media." *Journal of Infectious Diseases* 169: 1265–1270.

Facchini, P. J., K. L. Huber-Allanach, and L. W. Tari. 2000. "Plant Aromatic L-Amino Acid Decarboxylases: Evolution, Biochemistry, Regulation, and Metabolic Engineering Applications." *Phytochemistry* 54: 121–138.

Fones, H. N., D. P. Bebber, T. M. Chaloner, W. T. Kay, G. Steinberg, and S. J. Gurr. 2020. "Threats to Global Food Security From Emerging Fungal and Oomycete Crop Pathogens." *Nature Food* 1: 332–342.

Gnonlonfin, G. J. B., A. Sanni, and L. Brimer. 2012. "Review Scopoletin a Coumarin Phytoalexin With Medicinal Properties." *Critical Reviews in Plant Sciences* 31: 47–56.

Gross, G. G., J. Stöckigt, R. L. Mansell, and M. H. Zenk. 1973. "Three Novel Enzymes Involved in the Reduction of Ferulic Acid to Coniferyl Alcohol in Higher Plants: Ferulate: Co a Ligase, Feruloyl-Co a Reductase and Coniferyl Alcohol Oxidoreductase." *FEBS Letters* 31: 283–286.

Hawkins, C., B. Xue, F. Yasmin, G. Wyatt, P. Zerbe, and S. Rhee. 2025. "Plant Metabolic Network 16: Expansion of Underrepresented Plant Groups and Experimentally Supported Enzyme Data." *Nucleic Acids Research* 53: D1606–D1613.

He, B. T., Z. H. Liu, B. Z. Li, and Y. J. Yuan. 2022. "Advances in Biosynthesis of Scopoletin." *Microbial Cell Factories* 21: 152.

Heidarzadeh-Asl, S., M. Maurer, A. Kiani, D. Atiakshin, P. Stahl Skov, and D. Elieh-Ali-Komi. 2024. "Novel Insights on the Biology and Immunologic Effects of Histamine: A Road Map for Allergists and Mast Cell Biologists." *Journal of Allergy and Clinical Immunology* 155: 1095–1114.

Huang, H., Y. Li, J. Liang, and F. D. Finkelman. 2018. "Molecular Regulation of Histamine Synthesis." *Frontiers in Immunology* 9: 1392.

Jones, J., B. J. Staskawicz, and J. L. Dangl. 2024. "The Plant Immune System: From Discovery to Deployment." *Cell* 187: 2095–2116.

Jörnvall, H. 2008. "Medium- and Short-Chain Dehydrogenase/Reductase Gene and Protein Families: *MDR* and *SDR* Gene and Protein Superfamilies." *Cellular and Molecular Life Sciences* 65: 3873–3878.

Jun, S. Y., S. A. Sattler, G. S. Cortez, W. Vermerris, S. E. Sattler, and C. Kang. 2018. "Biochemical and Structural Analysis of Substrate

Specificity of a Phenylalanine Ammonia-Lyase." *Plant Physiology* 176: 1452–1468.

Jutel, M., M. Akdis, and C. A. Akdis. 2009. "Histamine, Histamine Receptors and Their Role in Immune Pathology." *Clinical and Experimental Allergy* 39: 1786–1800.

Kai, K., R. Wang, W. Bi, et al. 2021. "Chlorogenic Acid Induces ROS-Dependent Apoptosis in *Fusarium fujikuroi* and Decreases the Postharvest Rot of Cherry Tomato." *World Journal of Microbiology and Biotechnology* 37: 93.

Kanehisa, M., M. Furumichi, Y. Sato, M. Ishiguro-Watanabe, and M. Tanabe. 2021. "KEGG: Integrating Viruses and Cellular Organisms." *Nucleic Acids Research* 49: D545–D551.

Kelley, J. L., C. A. Miller, and H. L. White. 1977. "Inhibition of Histidine Decarboxylase. Derivatives of Histidine." *Journal of Medicinal Chemistry* 20: 506–509.

Kiedrowski, S., P. Kawalleck, K. Hahlbrock, I. E. Somssich, and J. L. Dangl. 1992. "Rapid Activation of a Novel Plant Defense Gene Is Strictly Dependent on the *Arabidopsis RPM1* Disease Resistance Locus." *EMBO Journal* 11: 4677–4684.

Kim, D. S., and B. K. Hwang. 2014. "An Important Role of the Pepper Phenylalanine Ammonia-Lyase Gene (*pal1*) in Salicylic Acid-Dependent Signalling of the Defence Response to Microbial Pathogens." *Journal of Experimental Botany* 65: 2295–2306.

Kim, S. J., K. W. Kim, M. H. Cho, V. R. Franceschi, L. B. Davin, and N. G. Lewis. 2007. "Expression of Cinnamyl Alcohol Dehydrogenases and Their Putative Homologues During *Arabidopsis thaliana* Growth and Development: Lessons for Database Annotations?" *Phytochemistry* 68: 1957–1974.

Kim, S. J., M. R. Kim, D. L. Bedgar, et al. 2004. "Functional Reclassification of the Putative Cinnamyl Alcohol Dehydrogenase Multigene Family in *Arabidopsis*." *Proceedings of the National Academy of Sciences of the United States of America* 101: 1455–1460.

Kollonitsch, J., A. A. Patchett, S. Marburg, et al. 1978. "Selective Inhibitors of Biosynthesis of Aminergic Neurotransmitters." *Nature* 274: 906–908.

König, S., K. Feussner, A. Kaever, et al. 2014. "Soluble Phenylpropanoids Are Involved in the Defense Response of *Arabidopsis* Against *Verticillium longisporum*." *New Phytologist* 202: 823–837.

Krell, T., J. A. Gavira, F. Velando, et al. 2021. "Histamine: A Bacterial Signal Molecule." *International Journal of Molecular Sciences* 22: 6312.

Kumar, R. 2016. "Evolutionary Trails of Plant Group II Pyridoxal Phosphate-Dependent Decarboxylase Genes." *Frontiers in Plant Science* 7: 1268.

Larroy, C., X. Parés, and J. A. Biosca. 2002. "Characterization of a *saccharomyces cerevisiae* NADP(H)-dependent Alcohol Dehydrogenase (ADHVII), a Member of the Cinnamyl Alcohol Dehydrogenase Family." *European Journal of Biochemistry* 269: 5738–5745.

Levine, R. J., and W. W. Noll. 1969. "Histidine Decarboxylase and Its Inhibition." *Annals of the New York Academy of Sciences* 166: 246–256.

Li, C., R. Jiang, X. Wang, Z. Lv, W. Li, and W. Chen. 2024. "Feedback Regulation of Plant Secondary Metabolism: Applications and Challenges." *Plant Science* 340: 111983.

Li, T., Q. Wang, R. Feng, et al. 2019. "Negative Regulators of Plant Immunity Derived From Cinnamyl Alcohol Dehydrogenases Are Targeted by Multiple *Phytophthora* Avr3a-Like Effectors." *New Phytologist*. https://doi.org/10.1111/nph.16139.

Li, Z., Y. Zhang, J. Ren, et al. 2022. "Ethylene-Responsive Factor ERF114 Mediates Fungal Pathogen Effector PevD1-Induced Disease Resistance in *Arabidopsis thaliana*." *Molecular Plant Pathology* 23: 819–831.

Liu, Q., L. Luo, and L. Zheng. 2018. "Lignins: Biosynthesis and Biological Functions in Plants." *International Journal of Molecular Sciences* 19: 335.

Liu, Y., Y. Y. Zheng, X. R. Zhou, et al. 2025. "Structural Insights Into the Role of RXLR Effectors in the Arms Race Between Oomycetes and Plants." *Molecular Plant Pathology* 26: e70138.

Maffei, M., C. Margherita Bertea, F. Garneri, and S. Scannerini. 1999. "Effect of Benzoic Acid Hydroxy- and Methoxy- Ring Substituents During Cucumber (*Cucumis sativus* L.) Germination. I.: Isocitrate Lyase and Catalase Activity." *Plant Science* 141: 139–147.

Mansell, R. L., G. G. Gross, J. Stöckigt, H. D. Franke, and M. H. Zenk. 1974. "Purification and Properties of Cinnamyl Alcohol Dehydrogenase From Higher Plants Involved in Lignin Biosynthesis." *Phytochemistry* 13: 2427–2435.

Montesano, M., H. Hyytiäinen, R. Wettstein, and E. T. Palva. 2003. "A Novel Potato Defence-Related Alcohol: $NADP^+$ Oxidoreductase Induced in Response to *Erwinia carotovora*." *Plant Molecular Biology* 52: 177–189.

Moriguchi, T., and J. Takai. 2020. "Histamine and Histidine Decarboxylase: Immunomodulatory Functions and Regulatory Mechanisms." *Genes to Cells* 25: 443–449.

Moya-García, A. A., A. Pino-Angeles, R. Gil-Redondo, A. Morreale, and F. Sánchez-Jiménez. 2009. "Structural Features of Mammalian Histidine Decarboxylase Reveal the Basis for Specific Inhibition." *British Journal of Pharmacology* 157: 4–13.

Naz, S., P. Liu, U. Farooq, and H. Ma. 2023. "Insight Into de-Regulation of Amino Acid Feedback Inhibition: A Focus on Structure Analysis Method." *Microbial Cell Factories* 22: 161.

Ngou, B., P. Ding, and J. Jones. 2022. "Thirty Years of Resistance: Zig-Zag Through the Plant Immune System." *Plant Cell* 34: 1447–1478.

Nguyen, G. T., Y. G. Kim, J. W. Ahn, and J. H. Chang. 2020. "Structural Basis for Broad Substrate Selectivity of Alcohol Dehydrogenase YjgB From *Escherichia coli*." *Molecules* 25: 2404.

Ninkuu, V., O. O. Aluko, J. Yan, et al. 2025. "Phenylpropanoids Metabolism: Recent Insight Into Stress Tolerance and Plant Development Cues." *Frontiers in Plant Science* 16: 1571825.

Ono, H. K., S. Hirose, K. Narita, et al. 2019. "Histamine Release From Intestinal Mast Cells Induced by Staphylococcal Enterotoxin A (Sea) Evokes Vomiting Reflex in Common Marmoset." *PLoS Pathogens* 15: e1007803.

Pick, A., B. Rühmann, J. Schmid, and V. Sieber. 2013. "Novel Cad-Like Enzymes From *Escherichia coli* K-12 as Additional Tools in Chemical Production." *Applied Microbiology and Biotechnology* 97: 5815–5824.

Prats, E., M. E. Bazzalo, A. León, and J. V. Jorrín. 2006. "Fungitoxic Effect of Scopolin and Related Coumarins on *Sclerotinia sclerotiorum*. A Way to Overcome Sunflower Head Rot." *Euphytica* 147: 451–460.

Qian, S., Y. Wang, and X. Zhang. 2019. "Inhibiting Histamine Signaling Ameliorates Vertigo Induced by Sleep Deprivation." *Journal of Molecular Neuroscience* 67: 411–417.

Ristaino, J. B., P. K. Anderson, D. P. Bebber, et al. 2021. "The Persistent Threat of Emerging Plant Disease Pandemics to Global Food Security." *Proceedings of the National Academy of Sciences of the United States of America* 118: e2115792118.

Saraiva, M., M. E. Ściślak, Y. T. Ascurra, et al. 2023. "The Molecular Dialog Between Oomycete Effectors and Their Plant and Animal Hosts." *Fungal Biology Reviews* 43: 100289.

Singh, S., C. Brocker, V. Koppaka, et al. 2013. "Aldehyde Dehydrogenases in Cellular Responses to Oxidative/Electrophilic Stress." *Free Radical Biology and Medicine* 56: 89–101.

Somssich, I. E., P. Wernert, S. Kiedrowski, and K. Hahlbrock. 1996. "*Arabidopsis thaliana* Defense-Related Protein ELI3 Is an Aromatic

Alcohol: NADP$^+$ Oxidoreductase." *Proceedings of the National Academy of Sciences of the United States of America* 93: 14199–14203.

Soviguidi, D. R. J., R. Pan, Y. Liu, L. Rao, W. Zhang, and X. Yang. 2021. "Chlorogenic Acid Metabolism: The Evolution and Roles in Plant Response to Abiotic Stress." *Phyton* 91: 239–255.

Stringlis, I. A., K. Yu, K. Feussner, et al. 2018. "Myb72-Dependent Coumarin Exudation Shapes Root Microbiome Assembly to Promote Plant Health." *Proceedings of the National Academy of Sciences of the United States of America* 115: E5213–E5222.

Tanaka, T., A. Ikeda, K. Shiojiri, et al. 2018. "Identification of a Hexenal Reductase That Modulates the Composition of Green Leaf Volatiles." *Plant Physiology* 178: 552–564.

Tang, Z., R. Mou, and G. Xu. 2025. "Defense Strategies for Plant Health: Disease Resistance and Tolerance." *Plant Cell* 37: koaf186.

Thévenot, E. A., A. Roux, Y. Xu, E. Ezan, and C. Junot. 2015. "Analysis of the Human Adult Urinary Metabolome Variations With Age, Body Mass Index, and Gender by Implementing a Comprehensive Workflow for Univariate and OPLS Statistical Analyses." *Journal of Proteome Research* 14: 3322–3335.

Thines, M. 2018. "Oomycetes." *Current Biology* 28: R812–R813.

Tsai, C. C., T. Y. Kuo, Z. W. Hong, et al. 2015. "*Helicobacter pylori* Neutrophil-Activating Protein Induces Release of Histamine and Interleukin-6 Through G Protein-Mediated MAPKs and PI3K/AKT Pathways in HMC-1 Cells." *Virulence* 6: 755–765.

Vanholme, R., B. De Meester, J. Ralph, and W. Boerjan. 2019. "Lignin Biosynthesis and Its Integration Into Metabolism." *Current Opinion in Biotechnology* 56: 230–239.

Wang, Y., Q. Cao, Q. Cao, et al. 2021. "Histamine Activates Hink to Promote the Virulence of *Pseudomonas aeruginosa*." *Science Bulletin* 66: 1101–1118.

Wang, Y., F. Govers, and Y. Wang. 2025. "Oomycete Plant Pathogens: Biology, Pathogenesis and Emerging Control Strategies." *Nature Reviews Microbiology*. https://doi.org/10.1038/s41579-025-01248-w.

Wu, F., J. Yu, and H. Gehring. 2008. "Inhibitory and Structural Studies of Novel Coenzyme-Substrate Analogs of Human Histidine Decarboxylase." *FASEB Journal* 22: 890–897.

Wu, M., Y. Li, Z. Liu, et al. 2024. "Genome-Wide Identification of the *CAD* Gene Family and Functional Analysis of Putative Bona Fide *CAD* Genes in Tobacco (*Nicotiana tabacum* L.)." *Frontiers in Plant Science* 15: 1400213.

Xu, X., H. Zhang, Y. Song, et al. 2012. "Strain-Dependent Induction of Neutrophil Histamine Production and Cell Death by *Pseudomonas aeruginosa*." *Journal of Leukocyte Biology* 91: 275–284.

Zhang, X., C. Fang, D. Huang, et al. 2021. "Determination of 8 Biogenic Amines in Aquatic Products and Their Derived Products by High-Performance Liquid Chromatography-Tandem Mass Spectrometry Without Derivatization." *Food Chemistry* 361: 130044.

Zhang, Z., W. Yang, T. Yuan, Y. Li, Q. Zhao, and Y. Dong. 2025. "Benzoic Acid Reduced Nutrient Absorption and Photosynthesis of Faba Bean to Promote *Fusarium* Wilt Occurrence." *Plant Disease* 109: 1551–1562.

Ziani, B. E. C., L. Barros, A. Z. Boumehira, et al. 2018. "Profiling Polyphenol Composition by HPLC-DAD-ESI/MSN and the Antibacterial Activity of Infusion Preparations Obtained From Four Medicinal Plants." *Food & Function* 9: 149–159.

Supporting Information

Additional supporting information can be found online in the Supporting Information section. **Figure S1:** Representative purification of AtCAD7. Lanes 1, *E. coli* crude extract; 2, molecular mass ladder; 3–9, fractions eluted from the metal chelate affinity column between 70 and 300 mM imidazole in Tris–HCl buffer. Proteins were visualised by Coomassie brilliant blue (CBB) staining. **Figure S2:** Validation of AtCAD7 enzymatic activity dependence on NADPH and reaction kinetics. (a) Enzymatic activity of AtCAD7 toward (Z)-3-hexenal, acrolein, and salicylaldehyde under different conditions: with NADPH (positive control), with NADH (coenzyme substitution), with heat-inactivated AtCAD7 (90°C for 10 min), and without AtCAD7 (no enzyme control). Assays were performed under standardised conditions (30°C, pH 6.5, 100 μM substrate, 200 μM coenzyme). Data represent mean ± SD of triplicate biological replicates. Statistical significance was assessed by Student's *t* test (**$p < 0.01$, ***$p < 0.001$). (b) Time-course analysis of AtCAD7-catalysed reduction of (Z)-3-hexenal, monitored by the change in absorbance at 340 nm (ΔA340) over 30 min. The reaction was carried out under standardised conditions with active AtCAD7 or without enzyme (control). **Figure S3:** Thin-layer chromatography of CAD7 reaction products. Enzymatic assays were performed as described in Materials and methods using purified CAD7 protein. Salicylaldehyde and methoxybenzaldehyde were used as substrates. TLC analysed each enzymatic reaction and standard 5 μL. Lanes 1, salicylaldehyde; 2, CAD7 enzymatic reaction of substrate salicylaldehyde (30 min); 3, salicyl alcohol; 4, 2-methoxybenzaldehyde; 5, CAD7 enzymatic reaction of substrate 2-methoxybenzaldehyde (30 min); 6, 2-methoxybenzyl alcohol. The chromatogram was visualised under UV 254 nm and documented photographically. **Figure S4:** Comparative analysis of substrate specificities for AtCAD7, its Arabidopsis homologues, and *E. coli* aldehyde reductases. (a) SDS-PAGE assay to confirm the integrity and purification of recombinant AtCAD5, AtCAD7, EcYahK and EcYjgB proteins. (b) Enzymatic activities of AtCAD7, AtCAD5, EcYahK, and EcYjgB toward (Z)-3-hexenal, acrolein, isovaleraldehyde, salicylaldehyde, and *p*-coumaryl aldehyde. No Substrate was negative control. Assays were conducted under standardised conditions (30°C, pH 6.5, 100 μM substrate, 200 μM NADPH). Data represent mean ± SD of triplicate biological replicates, demonstrating the differential substrate specificities of these enzymes. **Figure S5:** The OPLS-DA model validation for *AtCAD7*-silencing and *AtCAD7*-overexpression transformants. (a) The S-plots of the OPLS-DA analysis for OE7 (*AtCAD7*-overexpression) vs. WT and Ri7 (*AtCAD7*-silencing) vs. WT, respectively. The horizontal coordinates indicate the covariance between the principal components and metabolites, and the vertical coordinates indicate the correlation coefficients between the principal components and metabolites, the closer the metabolites are to the upper right and lower left corners, indicate more significant the differences are. The red points indicate the VIP values of these metabolites greater than or equal to 1, and the green points indicate the VIP values of these metabolites less than 1. (b) The horizontal coordinate represents the model accuracy, and the vertical coordinate represents the frequency of the model classification effect. The model conducted 200 random permutation experiments on the data. When $p = 0.02$ for Q^2, it indicates that there are 4 random grouping models with better prediction ability than the OPLS-DA model in this permutation test. When $p = 0.545$ for R^2Y, it means that there are 109 random grouping models with a better interpretation of the Y matrix than the OPLS-DA model in this permutation test. **Figure S6:** Functional analysis of histidine decarboxylase (HDC) in histamine biosynthesis, feedback regulation, and *P. parasitica* infection. (a) The inhibitory effect of histamine derived aldehydes on NbHDC protein in vivo using the plant histidine decarboxylase kit. The positive control was histamine-derived aldehydes (imidazole-4-carbaldehyde (IC) and 1-methylimidaz ole-4-carboxaldehyde (MC)), and the negative control was substrate solvent 2-methoxyethanol and Flag-GFP. Data are presented as mean ± SD (Student's *t*-test, $n = 3$, ***$p < 0.001$). (b) Quantification of histamine in *N. benthamiana* leaves overexpressing *GFP-NbHDC* or *Flag-GFP* (control) by LC–MS/MS. Values are presented as mean ± SD (Student's *t*-test, $n = 3$, **$p < 0.01$). (c) Agroinfiltration-mediated transient expression of *GFP-NbHDC* and *Flag-GFP* in *N. benthamiana*, followed by infection with *P. parasitica* zoospores at 2-day post-inoculation. The lesion development ($n \geq 15$) was scored at 2 dpi and *P. parasitica* biomass ($n = 3$) was quantified by genomic DNA qPCR assays. Error bars represent the standard deviation (SD), and asterisks indicate statistical significance based on a Student's *t*-test (*$p < 0.05$; **$p < 0.01$). (d) Western blot analysis to verify the expression and integrity of GFP-NbHDC and Flag-GFP fusion proteins. (e) Quantification of histamine in *AtCAD7*-overexpressing

(OE7) lines with or without histamine biosynthesis inhibitor treatment by LC–MS/MS. Values are mean ± SD (Student's *t*-test, $n = 3$, $^{**}p < 0.01$). **Figure S7:** Effects of histamine, scopolin, and chlorogenic acid on *P. parasitica* growth. (a) Growth of *P. parasitica* on CA medium after 72 h. Left to right: Untreated control; 20 μM histamine; 20 μM scopolin; 20 μM chlorogenic acid. Histamine treatment showed no significant effect on hyphal expansion compared to the control, whereas scopolin and chlorogenic acid markedly inhibited mycelial growth. Scale bar: 1 cm. Lesion diameters resulting from hyphal expansion are presented as mean ± standard deviation ($n = 3$). Statistical significance was determined using Student's *t*-test (ns, no significance; $^{*}p < 0.05$). (b) Hyphal morphology of *P. parasitica* under light microscopy. Left to right: untreated control showing normal hyphae; histamine-treated hyphae no observable morphological alterations; scopolin and chlorogenic acid treated hyphae exhibiting severe distortion. Scale bars: 250 μm and 500 μm. **Figure S8:** Expression of phenylpropanoid-related genes in *Arabidopsis thaliana* in response to *Phytophthora parasitica* infection. (a–c) The expression of phenylpropanoid-related genes *PAL1* (a), *C3′H* (b), and *F6′H1* (c) in response to *P. parasitica* infection at different time points (hours post-inoculation, hpi) were examined, with the *AtUBC9* gene as an internal control. Results are presented as the mean ± SD of three biological repeats (three leaves from different plants were collected together as one repeat). Statistical significance was assessed by Student's *t* test. $^{*}p < 0.05$, $^{**}p < 0.01$, ns, not significant. Similar results were observed in two independent experiments. **Table S1:** List of the top 20 metabolites of differential metabolites between OE7 lines and wild type with their names, mass/charge ratio, molecular formula, class, VIP, and fold change. The metabolites were ranked by VIP values. **Table S2:** List of the top 20 metabolites of differential metabolites between Ri7 lines and wild type with their names, mass/charge ratio, molecular formula, class, VIP, and fold change. The metabolites were ranked by VIP values. **Table S3:** Primers used in this study.